Fission decay of $N = Z$ nuclei at high angular momentum: ^{60}Zn

W. von Oertzen,[1,2,*] V. Zherebchevsky,[1,3] B. Gebauer,[1] Ch. Schulz,[1] S. Thummerer,[1] D. Kamanin,[4] G. Royer,[5] and Th. Wilpert[1]

[1]*Hahn Meitner Institut GmbH, Glienicker Strasse 100, D-14109 Berlin, Germany*
[2]*Fachbereich Physik, Free University of Berlin, Germany*
[3]*St. Petersburg University, St. Petersburg, Russia*
[4]*FLNR, JINR, Dubna, Russia*
[5]*Laboratoire Subatech, Université-IN2P3/CNRS-Ecole des Mines, F-44307 Nantes, France*

(Received 15 November 2007; published 17 October 2008)

Using a unique two-arm detector system for heavy ions (the BRS, binary reaction spectrometer), coincident fission events have been measured from the decay of ^{60}Zn compound nuclei formed at 88 MeV excitation energy in the reactions with ^{36}Ar beams on a ^{24}Mg target at $E_{\rm lab}(^{36}{\rm Ar}) = 195$ MeV. The detectors consisted of two large-area position-sensitive (x, y) gas telescopes with Bragg-ionization chambers. From the binary coincidences in the two detectors, inclusive and exclusive cross sections for fission channels with differing losses of charge were obtained. Narrow out-of-plane correlations corresponding to coplanar decay are observed for two fragments emitted in binary events, and in the data for ternary decay with missing charges from 4 up to 8. After subtraction of broad components, these narrow correlations are interpreted as a ternary fission process at high angular momentum through an elongated shape. The lighter mass in the neck region consists dominantly of two or three α particles. Differential cross sections for the different mass splits for binary and ternary fission are presented. The relative yields of the binary and ternary events are explained using the statistical model based on the extended Hauser-Feshbach formalism for compound nucleus decay. The ternary fission process can be described by the decay of hyper-deformed states with angular momenta around $4552\hbar$.

DOI: 10.1103/PhysRevC.78.044615 PACS number(s): 25.70.Jj, 24.60.Dr, 25.70.Pq, 27.50.+e

I. INTRODUCTION

For nuclei with masses ranging from $A = 40$ up to 100 at high angular momentum, "exotic" shapes called super- and hyper-deformed are predicted within various theoretical approaches [1–7]. For these nuclei, fission decay is expected to proceed through shapes with large deformations, in particular for the large angular momenta. Some authors have indicated that the structure of the fissioning nucleus at the saddle point is strongly determined by clustering [3,5], which can influence the fission decay modes with cluster emission. Studies of the binary decays, as well as cluster emission of such compound nuclei (CN) in the mass region $A = 40$–60, have been reported in the last two decades [8–12].

The most important factors governing fission decay can be described by the two fissility parameters η_i, which determine the neck formation [1]. The parameter η_x is used as a measure of the relative strength of two competing forces due to the Coulomb energy (repulsive) and the surface energy (attractive), and further the parameter η_y is introduced to describe the relative strength of the centrifugal energy (repulsive) determined by the angular momentum L and the surface energy (attractive). For nuclei of mass A, charge Z, and radius R, these parameters are given by

$$\eta_x = \frac{E_{\rm Coul}}{2E_{\rm Surf}} = C_x \frac{Z^2}{A}, \quad \eta_y = \frac{E_{\rm Rot}}{E_{\rm Surf}} = C_y \frac{L^2}{AR^4}, \qquad (1)$$

with two constants C_x and C_y, respectively. For large values of the fissility parameter, $\eta_x = 0.7$–0.8, in heavy nuclei, the saddle point configurations are predicted [1] to be very compact, no real neck is formed. The quadrupole deformation parameter β_2 at the saddle point may be in the range of only 0.2–0.3. In contrast, for small values of the fissility parameter, $\eta_x = 0.3$–0.4, for light nuclei as in our case, the configurations of the saddle point are predicted to become very elongated [1,2] with decreasing fission parameter. For nuclei in the mass region of $A = 56$–100, a ternary fission process is expected to occur. Furthermore, the neck becomes longer and "thicker" at higher angular momenta, i.e., with increasing values of the second fissility parameter η_y. For the excited states in light $N = Z$ nuclei at high angular momentum, super-deformed and very elongated hyper-deformed shapes are predicted, stabilized by special quantal shell effects [3–7]. In these nuclei ($A =$ 40–100), energetically favored states with super- and hyper-deformed shapes with quadrupole deformation parameters $\beta_2 = 0.6$–1.0 (with 2:1 and 3:1 as ratios between the major to minor axis for ellipsoidal deformation, respectively) and even larger values are predicted with the Nilsson-Strutinsky method [5–7]. The well-established shell corrections will stabilize the rotating CN in its hyper-deformed shape at high angular momentum [6]. Alternatively, hyper-deformed configurations are also obtained in an α-cluster model [3], a fact which gives strong indications for the relation between large deformations and clustering. From these results, it can be anticipated that in the mass region of the present work ($A = 50$–60) the super- and hyper-deformed states at high angular momentum will have fission as one of the dominant decay modes [11,13]).

*oertzen@hmi.de

The ternary fission process is strongly enhanced for the configurations with the largest deformations due to the large moments of inertia and the corresponding lowering of the fission barrier, which in addition can be decreased by the mentioned shell corrections. In another approach, using a generalized liquid-drop model, taking into account the proximity energy and quasimolecular shapes (as in the cluster models), Royer *et al.* [14,15] have also predicted several of such ternary fission modes in ^{56}Ni and ^{48}Cr compound nuclei. In these systems, even macroscopically super- and hyper-deformed minima appear at the foot of the potential fission barrier at sufficiently high angular momenta. However, until now, experimental evidence for such ternary breakup of the light nuclei has not been reported (e.g., Ref. [16]). Previous reports on the results of the present work are contained in Refs. [17–20], and the most recent work on ^{56}Ni in Ref. [21]. Work on fission in a similar mass range has been described in Refs. [9–11]. Ternary fission in the statistical approach has been discussed in a recent study also for ^{56}Ni [13].

II. DETECTOR SYSTEM BRS

The present experiment has been performed with the binary reaction spectrometer (BRS) in combination with the γ-detector array OSIRIS at the HMI (Berlin) with a ^{36}Ar beam of 195 MeV [22,23]. A similar experiment has been performed with a ^{32}S beam in the BRS-Euroball-IV campaign [20]. The experimental setup is shown in Fig. 1. In these experiments, coincidences of γ rays (with the OSIRIS array) with charged fragments have been used for γ spectroscopy. Two heavy fragments are registered in kinematic coincidence and identified by their charge in two large-area position-sensitive Bragg ionization chambers (BICs) [24]. Two detector telescopes labeled 3 and 4 (Det3 and Det4) are placed symmetrically to the beam axis and consist of two-dimensional position-sensitive low-pressure multiwire chambers (MWCs) and Bragg-curve ionization chambers. All detection planes are electrically fourfold segmented, in order to improve the resolution and counting rate capabilities. The scheme in Fig. 2 shows the arrangement of the position-sensitive part and the BICs. The parameters giving the identification of the fragments by their charge are the Bragg peak height BP, the range R, and the rest energy E. Their momentum vectors are obtained through the position signals (x and y) of the two telescopes, from which the angles in the reaction plane, θ, and out-of-plane, ϕ, are determined, see Fig. 3.

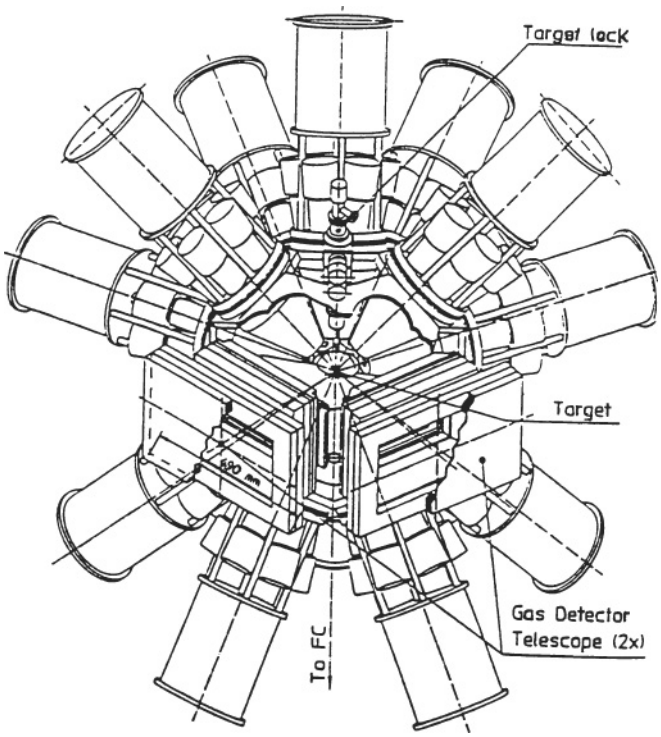

FIG. 1. BRS-OSIRIS setup used for the study of coincident fission channels in the reactions $^{36}\mathrm{Ar} + {}^{24}\mathrm{Mg} \rightarrow Z_3 + Z_4 + \Delta Z$, at $E_{\mathrm{lab}}(^{36}\mathrm{Ar}) = 195$ MeV. The OSIRIS γ-detector array consisted of 12 Compton-suppressed Ge detectors.

With the BRS, it is therefore possible to measure two heavy fragments in coincidence with respect to their in-plane (θ_3, θ_4) and out-of-plane (ϕ_3, ϕ_4) scattering angles, time of flight (TOF) and energy E. Compared to previous works, these coincidences represent an exclusive measurement of the binary fission yield. More detector details can be seen in Fig. 2; see also Ref. [17]. The angular ranges of the two detectors cover a very large solid angle of twice 156 msr ($\Delta\theta = 12^\circ$–46°, $\Delta\phi = 2 \times 17.4^\circ$). Examples of BP vs E and R spectra are shown later in Figs. 5 and 6. The inclusive yields are obtained by setting just Z gates in either one of the detectors. For the exclusive detection of "binary" exit channels, two heavy fragments in coincidence are considered, with a definite choice of the charge registered in Det3 and Det4. A survey of the reaction channels and their Q values is given in Fig. 4. For the discussion of the reaction channels with two heavy ejectiles, the angular correlations with the in-plane θ and out-of-plane ϕ angles are the most relevant.

III. EXPERIMENT

A. General experimental conditions

The reaction studied in the present work can schematically be written as $(M_1, Z_1) + (M_2, Z_2) \rightarrow {}^{60}\mathrm{Zn}^* \rightarrow (M_3, Z_3) + (\Delta Z) + (M_4, Z_4)$. Two heavy fragments with masses (M_3, M_4) and charges (Z_3, Z_4) are registered in kinematic coincidence and identified by their charges. The masses could not be fully determined in these experiments; however, a mass resolution of 3–4 mass units was obtained by the timing signals of the MWC against the beam pulses (1–3 ns), see Refs. [17,19]. We have investigated the fission decay of the ^{60}Zn CN with the excitation energy of 88 MeV and a maximum value of the angular momentum in the range of 44–52$\hbar$. A similar system, $^{32}\mathrm{S} + {}^{24}\mathrm{Mg}$, has been studied with the BRS-Euroball setup, and a detailed report is in preparation [20]. The latter system has also been studied extensively by Sanders *et al.* [9–11], with the emphasis on the inclusive fusion cross section, the binary fission process identified using kinematic coincidences. From this pioneering work, some basic information for the CN formation in the present reactions can be determined. For instance, the maximum

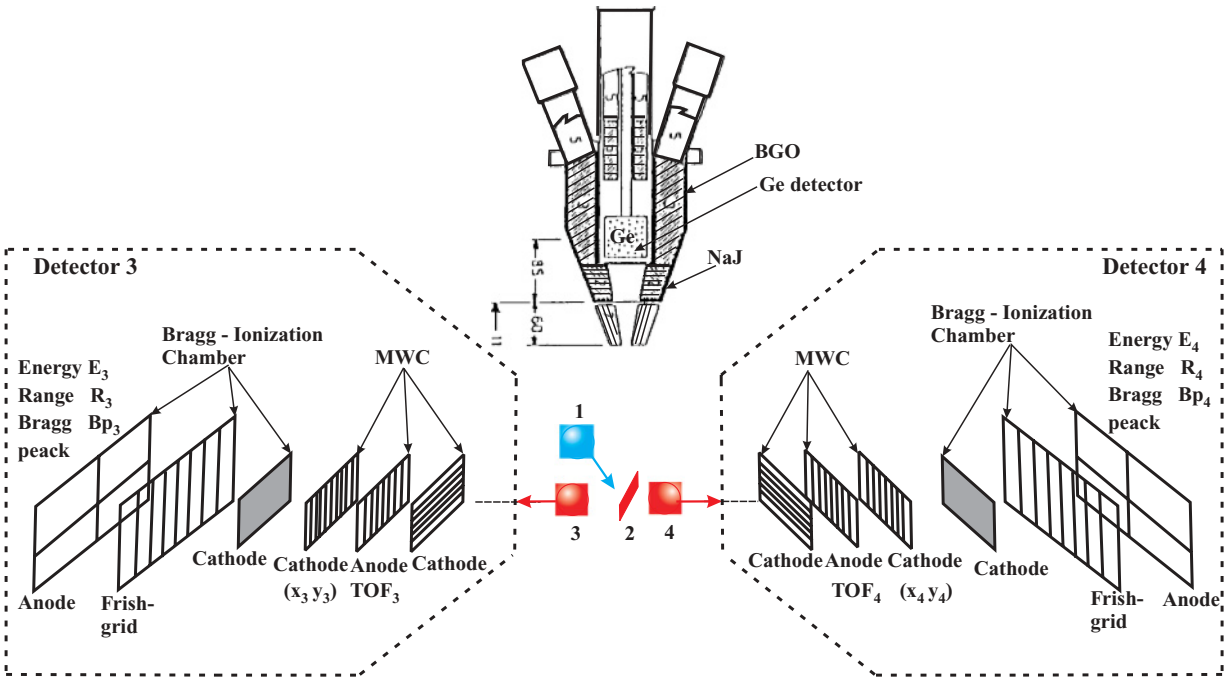

FIG. 2. (Color online) Schematic representation of the telescopes of the BRS with one cluster-γ detector of the OSIRIS array. The position-sensitive (x, y) low-pressure MWC and the BIC are indicated.

angular momentum reached for ^{56}Ni is close to 45$\hbar$, consistent with the predicted liquid-drop limit [25]. At these highest angular momenta, the binary fission decay contributes up to 10% of the total fusion cross section. It will be shown that the ternary fission decay in these nuclei competes with the binary fission because of the large moments of inertia of the elongated shapes in the saddle point and the possible formation of hyper-deformed configurations.

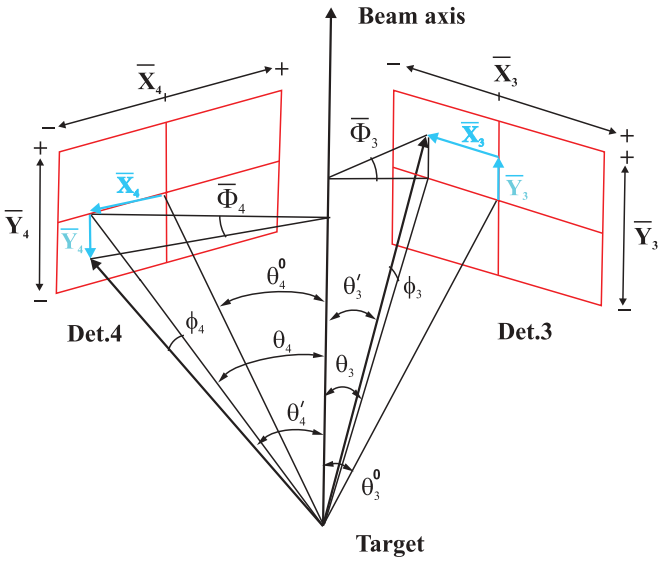

FIG. 3. (Color online) Definitions of the in-plane (θ_3, θ_4) and out-of-plane (ϕ_3, ϕ_4) scattering angles obtained from the $\overline{X}$ and $\overline{Y}$ readouts of the position-sensitive detectors.

We have observed binary coincidences, channels defined by $Z_3 + Z_4$, with increasing loss of light particles, $\Delta Z (Z_{CN} - \Delta Z = Z_3 + Z_4)$, the Q values of these reactions are summarized in Fig. 4. The values become rather negative for larger ΔZ. We have selected binary and nonbinary channels by choosing a Z gate in one detector (Det4, Z_4) and collecting all coincident charge yields in the second detector (Det3, Z_3). The corresponding yields in the Bragg peak (BP) vs energy and the Bragg peak vs range (R) distributions are shown in Figs. 5 and 6, respectively. This procedure gives the *inclusive* binary yields, which are shown in Fig. 7.

Choosing a second gate in Det3, we obtain the *exclusive* reaction channels for the sum of the charges ($Z_3 + Z_4$). This procedure defines channels with a fixed missing charge, in the range $\Delta Z = 0$–8. These exclusive yields are the subject of the detailed discussions in Secs. III and IV.

The missing charges can be evaporated (statistical decay) from the excited fragments in binary fission which gives broad distributions for the in-plane and out-of-plane correlations. If the missing charges are left with some smaller residual momentum between the two heavy fragments, we will refer to this process as ternary fission, see Fig. 8. The latter will give sharp correlations perpendicular to the reaction plane (coplanarity). The reaction plane is spanned by the beam axis and the vectors of the two fragments in Det3 and Det4, with charges Z_3, Z_4. For the following discussion, the coplanarity condition is of importance. We define coplanarity with the relation for the out-of-plane angles $(\phi_3 - \phi_4) = 180^\circ$. The out-of-plane correlations $N(\phi_3, \phi_4)$ of the selected events are uniquely determined with the BRS-detector system over a very wide angular range in the reaction plane (θ). These fragment yields $N(\phi_3, \phi_4)$ are very important for the later discussion.

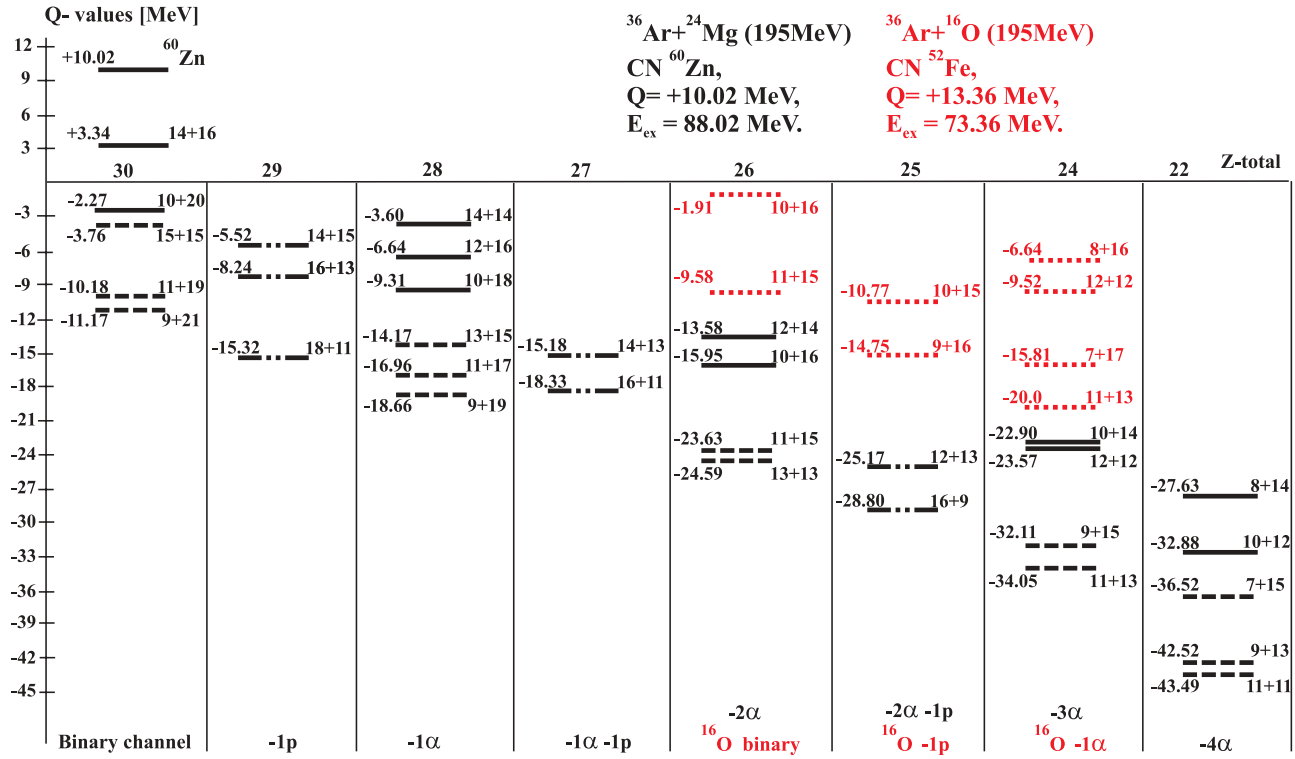

FIG. 4. (Color online) Q values for different binary and nonbinary decay channels for the compound nuclei ^{60}Zn and ^{52}Fe, defined by the charges $Z3$ and $Z4$ ($Z3 + Z4$) as indicated. The values are given for the even missing charges (missing number of α particles) and for odd missing charges (missing number of protons p and $x\alpha$ particles) as indicated in the bottom line.

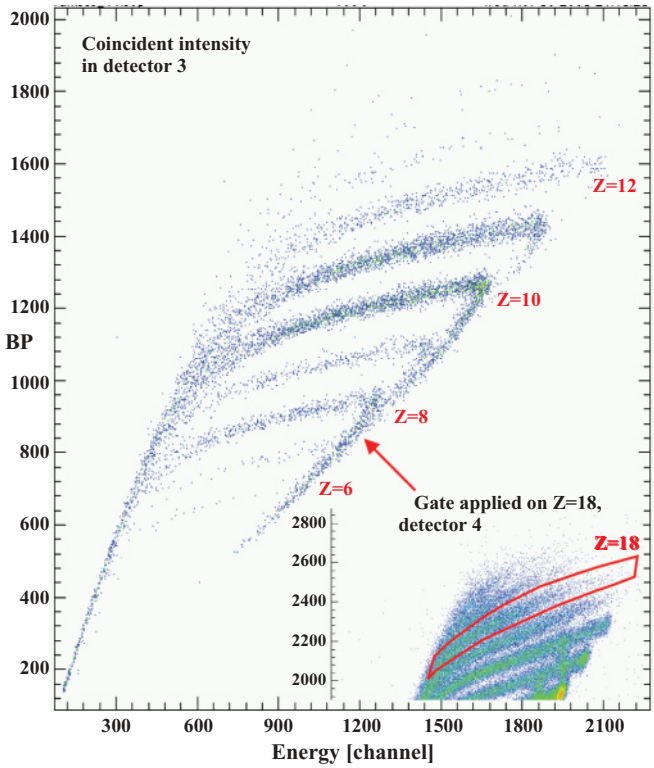

FIG. 5. (Color online) Bragg peak (BP) vs energy distributions of the events in the Det3, obtained in coincidence with a gate set for $Z = 18$ in Det4 (insert), for the reaction $^{36}\mathrm{Ar} + {}^{24}\mathrm{Mg} \rightarrow Z_3 + Z_4 + \Delta Z$.

The target consisted of 100 μg/cm^2 of ^{24}Mg enriched to 99.9% on a layer of 20 μg/cm^2 of ^{12}C. The compound nuclei ^{60}Zn are formed at an excitation energy of $E_{\mathrm{ex}} =$ 88 MeV at a bombarding energy of $E_{\mathrm{lab}}(^{36}\mathrm{Ar}) = 195$ MeV. The experiment performed at the HMI Berlin and the BRS had rather good vacuum conditions. Binary coincidences of the two BRS detectors were registered with at least one γ ray in coincidence in the OSIRIS array. The data have already been partially published in Refs. [17–19].

B. Experimental results

Charge separation has been obtained in the BICs. The reaction channels are defined using corresponding gates on the BP-E distributions for the different charges; thus a large variety of $(Z_3 + Z_4)$ combinations are observed with their corresponding correlations in angles ϕ and θ. The individual binary and nonbinary reaction channels can be clearly defined in this way. The total kinetic energy (TKE) is the sum of the energies of the registered fragments. To judge the efficiency of the channel selection, we show the inclusive yields in Fig. 7 with the two choices of the primary gate either in Det3 or Det4. The differences between the two distributions are due to the uncertainties in the limits of the gates at the lower energies. For different charge (mass) asymmetries there are also differences in the coincident angular acceptance in the θ ranges in the laboratory system. The falloff of the intensities

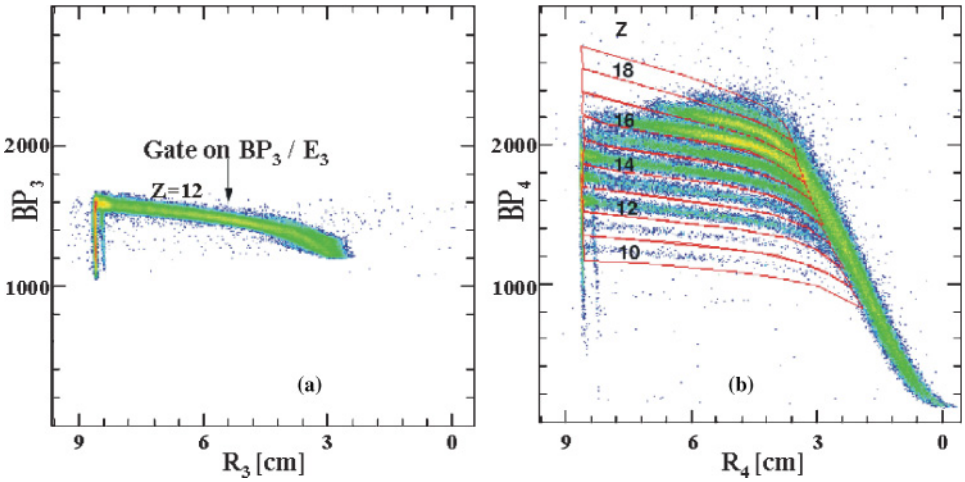

FIG. 6. (Color online) Bragg peak (BP) vs range (R_i) distributions of the events in Det4, panel (b), obtained in coincidence with a gate set for Z identification in Det3, panel (a), for the reaction $^{36}\mathrm{Ar} + {}^{24}\mathrm{Mg} \rightarrow Z_3 + Z_4 + \Delta Z$.

for large asymmetries is thus due to the loss in efficiency of registration (e.g., Figs. 18 and 19 in Sec. IV B).

A narrow distribution with $(\phi_3 - \phi_4) = 180^\circ$ uniquely defines the missing momentum in the reaction plane spanned by the beam direction and the vectors of the two heavy fragments. For $\Delta Z = 4, 6$ these narrow out-of-plane distributions define coplanar (or collinear) ternary fission with a small out-of-plane momentum. As will be discussed later, the decay of the elongated CN at high angular momentum favors a collinearity of the fragments.

For the determination of the kinetic energy of the fragments, a method for the energy calibration has been developed. The general idea of the method is a transformation of the residual energy of the fragments in the BIC into their initial energy by using an analysis based on the calculation of the Bragg curves. The fragments are not fully stopped in the Bragg chamber, and for smaller charges, 16 ascending and descending branches are obtained. The new aspect of this procedure is the calculation of the mentioned branches of the Bragg curves to get the full energy information. The calibration procedure included several steps.

First, energy loss calculations for each charge were made with the identification of the punch-through point. By using the code EVER (Energieverlust Rechnungen) the energy that was lost by the fragments on the way from the target to BIC was calculated. Then the energy of the fragments deposited in the Bragg chamber as a function of the initial energy of the fragments was plotted for each charge (see Fig. 9).

Next, we searched for the punch-through points in our experimental results (use of the Bragg peak vs energy distributions). Setting gates on the back-bend region in the BP-E distributions, we get the energy spectra for different charges which contain the experimental punch-through point. The experimental BP-E distributions are divided into two branches: ascending and descending. The gates for the charges in the BP-E distributions were set in accordance with the cuts for two different branches (ascending and descending) in the range-Bragg peak distributions (for more detail, see Ref. [19]). A typical energy spectrum after this calibration procedure is shown in Fig. 10. To estimate the uncertainty, we compared the experimental maximum values of TKE for some combinations of (Z_3, Z_4) with kinematic calculations and found that the experimental absolute values are typically 6–7 MeV too low. This effect is due to the energy loss calculations with differing values of the energy losses in the gas (which depend on temperature) and in the foils. The relative values have a much smaller uncertainty, of less than 1 MeV. These considerations are also relevant for the discussion in Sec. V B.

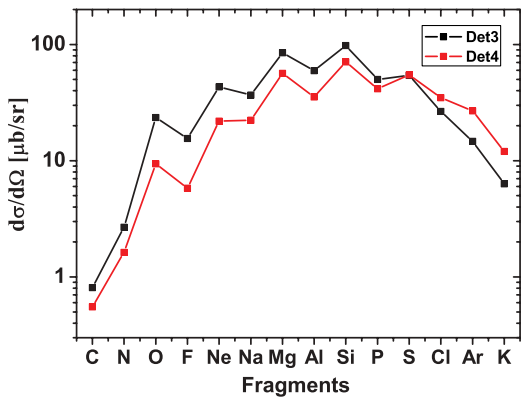

FIG. 7. (Color online) Inclusive coincidence yields, obtained with a gate set for Z identification in either Det3 or Det4 for the reaction $^{36}\mathrm{Ar} + {}^{24}\mathrm{Mg} \rightarrow Z_3 + x$ or $Z_4 + x$, for an angular range of $\theta_{\mathrm{c.m.}} = 65^\circ$–$120^\circ$.

Using the present method of the energy calibration, the TKEs (the sum $E_3 + E_4$) of the fragments were obtained and two-dimensional TKE vs $(\phi_3 - \phi_4)$ distributions were built (see Figs. 11 and 12). The TKE values do not appear in an absolute scale because of some remaining problems with the energy calibration of the BIC.

The TKE is shown as function of $(\phi_3 - \phi_4)$ for a pair of coincident charges Z_3, Z_4 with different combinations for the condition $(Z_3 + Z_4 =$ even or odd). The same coincident fragment yields, $N(Z_3, Z_4)$, are shown in Fig. 13 as a projection on $(\phi_3 - \phi_4)$. The distributions are fitted by Gaussians and the full widths at half maximum (FWHM) are given in the figure.

In the first row of Figs. 11 and 13, we have the purely binary decay processes ($\Delta Z = 0$) with exit channels corresponding to different asymmetry of the charges. For purely binary

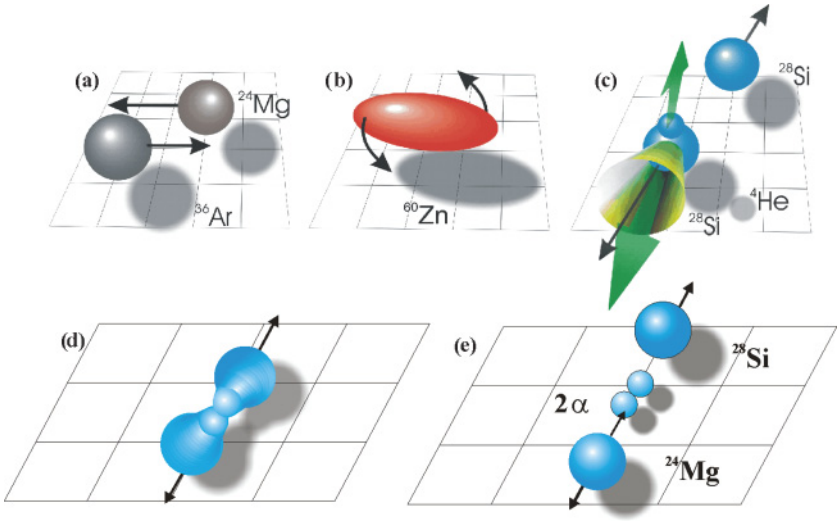

FIG. 8. (Color online) Binary and ternary fission processes from possible hyper-deformed states in the ^{60}Zn CN with α-cluster emission from the binary fragments (c), or with the formation of α clusters in the neck (d), (e), respectively.

($\Delta Z = 0$) events, narrow distributions around $(\phi_3 - \phi_4) = 180^\circ$ are indeed observed, a small wider contribution results from the evaporation of neutrons. No narrow distribution is observed for $\Delta Z = 1, 2$. These events are originally binary fission with an excitation energy in either fragment sufficiently high for a proton or one α particle to be emitted. The distributions become wider with increasing number of missing α particles, the systematics of the widths are shown in Fig. 13. We can easily identify the broad yields as binary fission with increasing excitation energy in each primary fragment and the evaporation of 1–4α particles, respectively. The Q values allow the decay with $\Delta Z = 8$, see Fig. 13; however, these yields are very small. For asymmetric mass splits, the coincident events move out of the angular acceptance in (θ_3, θ_4). An example of these correlations is given later in Fig. 19.

In the second row ($\Delta Z = 2$), we observe the highest yield, with a wide out-of-plane spectrum. For this particular case, a fit by two different Gaussian distributions (the first with the same width as for $\Delta Z = 0$) gives a clear indication that a small narrow component exists in these channels (similar to the narrow parts observed for the larger ΔZ). The contribution of the narrow parts with a width as in the binary case is here about 2%, the experimental "narrow" part from neutron evaporation is about 9–10% of the total yield.

In the other rows, with the coincidences for ($\Delta Z = 2, 4, 6, 8$), the (ϕ_3, ϕ_4) correlations show an increasing width with larger charge losses, the broad component being located at lower TKE. This corresponds to the expectation of a sequential uncorrelated statistical emission of several charged particles from the excited fragments. However, for $\Delta Z = 4$, which corresponds to two missing α particles (third row in Figs. 11 and 13), a strong narrow component as in the binary cases is observed together with the broad component. The pattern of narrow correlations continues to appear for three missing α articles, where again two components, a narrow peak (as in the binary event) and a wider distribution, Fig. 11 and Fig. 13, fourth row) are observed. For the case of four missing α particles, the Q values are extremely negative, but again both components are visible (Fig. 13).

We also show the yields, TKE-$(\phi_3 - \phi_4)$, for cases with an odd missing charge ($Z3 + Z4 = \text{odd}$), see Figs. 12 and 15. These correspond to an additional loss of a proton. The yields are lower because of the more negative Q values. We note

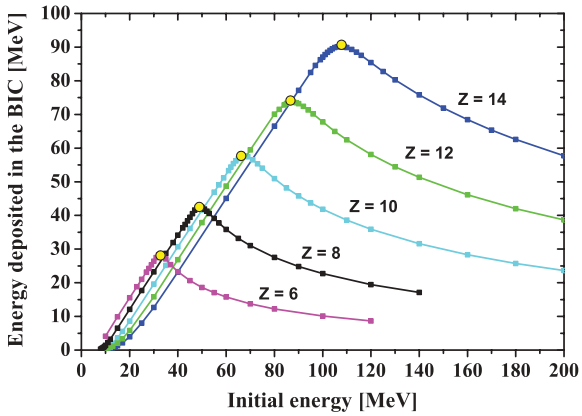

FIG. 9. (Color online) Energy deposited by fragments in the BIC as a function of their initial energy and the determination of the punch-through points (circles).

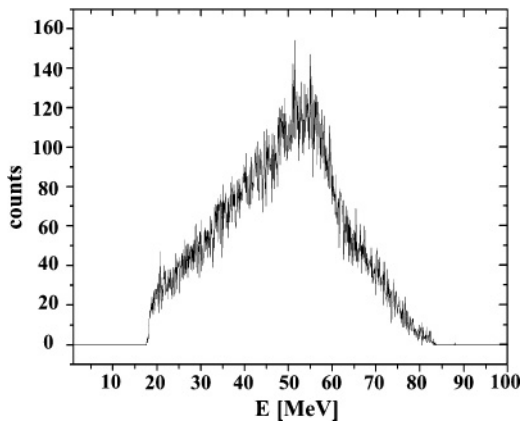

FIG. 10. Energy spectrum of the ^{16}O nuclei registered in Det3, obtained with the calibration procedure.

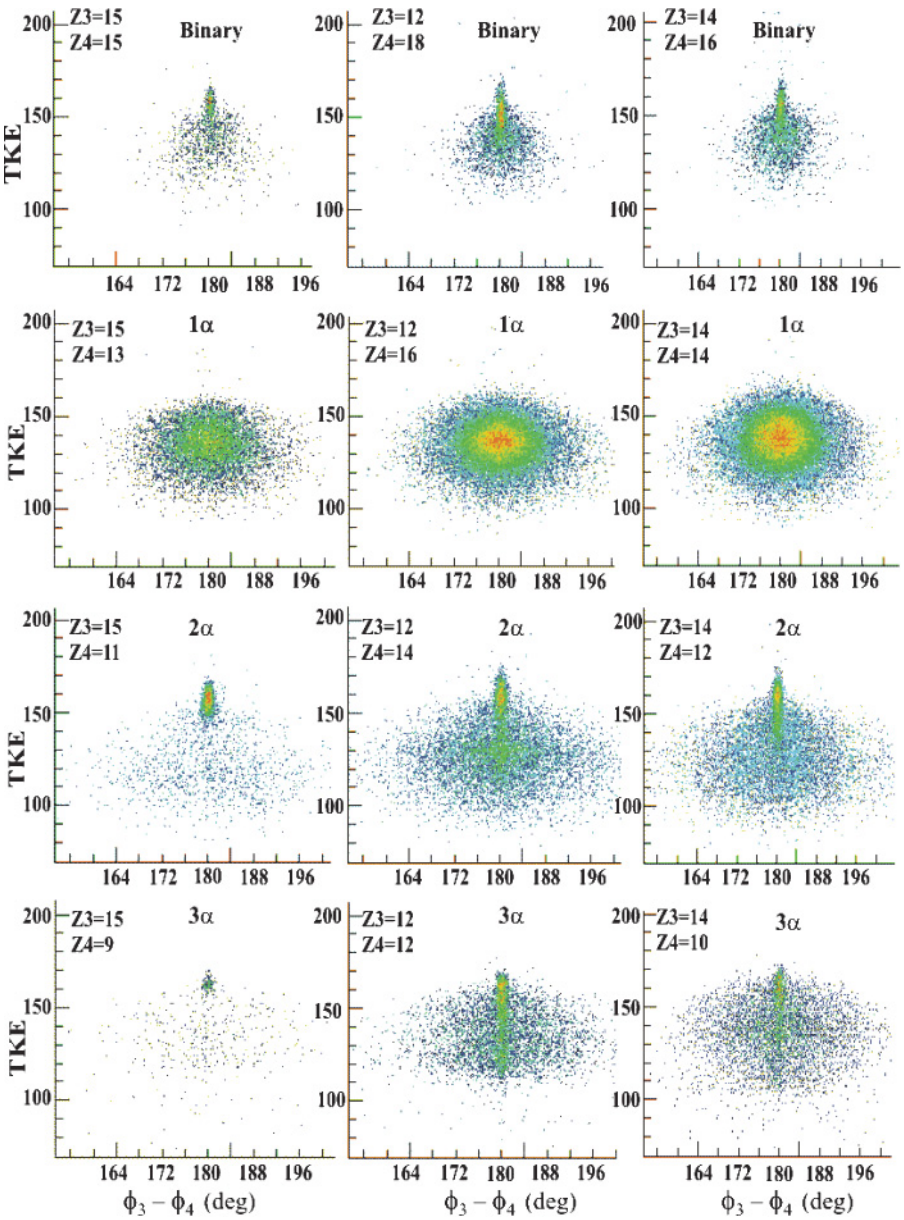

FIG. 11. (Color online) Two-dimensional plots of TKE in MeV (not in an absolute scale) as function of the out-of-plane angles ($\phi_3 - \phi_4$) in degrees, for two coincident fragments for which the sum of the charges $Z3$ and $Z4$ is even; the missing number of α particles is also indicated.

similar systematics: the $-1p$ yields show clearly the effect of the statistical emission, the yields with $(-1\alpha, -1p)$ are again wider. However, only a small component appears in the channels with the loss of $(2\alpha + 1p)$, which have quite unfavorable Q values for the ^{24}Mg target. The main yield at the higher TKE in these channels (bottom row in Fig. 12) will originate from reactions on ^{16}O in the target, where it corresponds to the $(-1p)$ channel with a much more favorable Q value (see Q values in Fig. 4). This yield, in comparison with those of the first row, allows the determination of the ^{16}O in the target, discussed in detail in Sec. IV.

IV. ANALYSIS OF THE DATA

A. Out-of-plane correlations and target contaminants

The out-of-plane correlations allow a direct distinction between binary and coplanar ternary decays. For the narrow component, we have to discuss the contribution from contaminants in the target. This is a very important question, because the effect observed in the out-of-plane distributions for $(-2\alpha, \Delta Z = 4$ and $-3\alpha, \Delta Z = 6)$ could be explained as a binary decay of a compound system formed with ^{16}O or ^{12}C instead of ^{24}Mg. In the present case, it will be the ^{36}Ar + ^{16}O reaction (CN = ^{52}Fe) for the $\Delta Z = 4$ channel, and the ^{36}Ar + ^{12}C reaction (CN = ^{48}Cr) for the $\Delta Z = 6$ channel. Therefore the probability of the reactions with ^{16}O and ^{12}C nuclei has been estimated. The following several points show that the contributions from ^{16}O or ^{12}C in the target are only 15–20%.

1. Estimations of the absolute ^{16}O target thickness. For the target thickness determination of the ^{16}O component, we assume that the differential fission cross section for the narrow part, binary for ^{16}O (with missing charge $\Delta Z = 4$), to be the same as the differential fission cross section for the pure binary decay with $\Delta Z = 0$ for CN = ^{60}Zn. If the narrow peak in the out-of-plane distribution for the $\Delta Z = 4$ case arises only

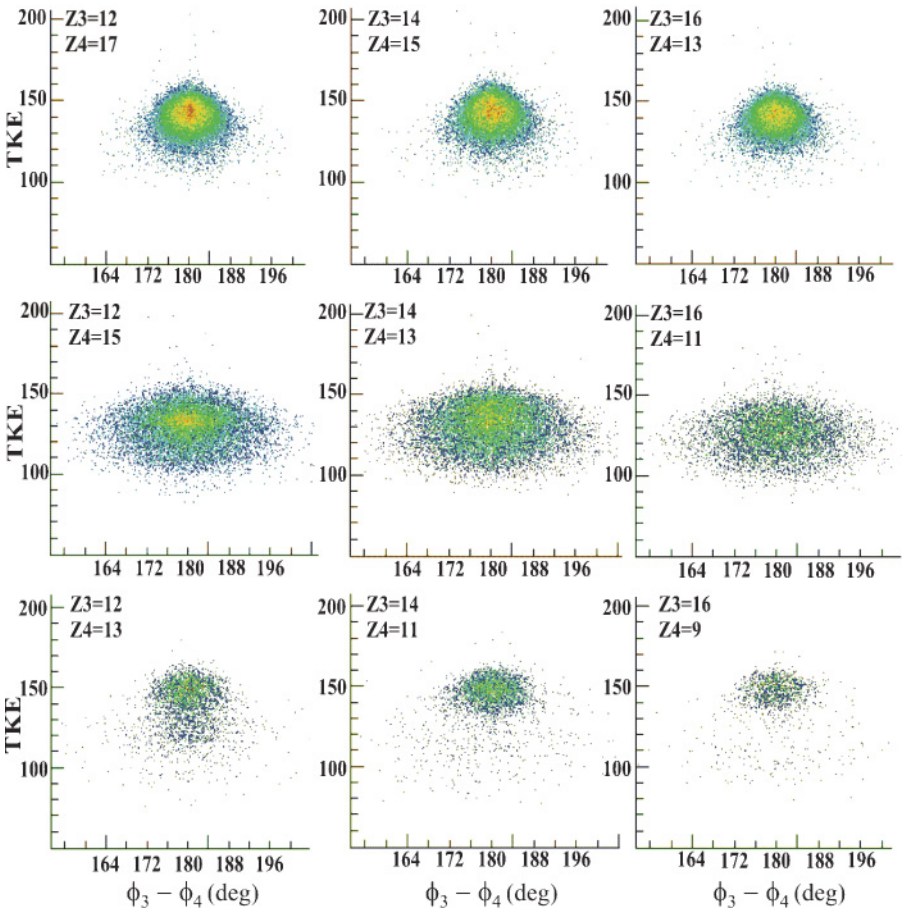

FIG. 12. (Color online) Same as Fig. 11, but the sum of the charges ($Z3 + Z4$) is odd. The missing numbers of α particles and protons are, from the top, $(-1p)$, $(-1p, -1\alpha)$, and $(-1p, -2\alpha)$.

because of reactions on ^{16}O, with the same differential cross section for fission for both cases, we need two times more ^{16}O than is possible for a completely oxidized ^{24}Mg target (only a 10% oxidation is expected). The vacuum in the BRS system was below 10^{-6} mbar in the present experiment.

2. Analysis of the ratios of the differential cross sections for the binary ($\Delta Z = 0$) to the $\Delta Z = 2$ charge combinations. From the out-of-plane distributions [see Fig. 14(a)], we have calculated the ratio $R(1\alpha/\alpha)$, in the c.m. system of the differential cross sections of the binary fission with 1α emission ($^{36}\mathrm{Ar} + {}^{24}\mathrm{Mg} \rightarrow {}^{60}\mathrm{Zn} \rightarrow {}^{28}\mathrm{Si} + {}^{28}\mathrm{Si} + 1\alpha$) to the differential cross section of the pure binary process ($^{36}\mathrm{Ar} + {}^{24}\mathrm{Mg} \rightarrow {}^{28}\mathrm{Si} + {}^{32}\mathrm{S}$). The same value is assumed for this ratio for the decay of the CN = ^{52}Fe (the ^{16}O target). We find that the yield in the broad distribution $\Delta Z = 2$, is eight times stronger [Fig. 14(b)] than the yield of the pure binary ($\Delta Z = 0$) decay, $R(1\alpha/0\alpha, {}^{60}\mathrm{Zn}) = 8$. Applying this value to the narrow part in $\Delta Z = 4$ with the contaminant, for $^{36}\mathrm{Ar} + {}^{16}\mathrm{O} \rightarrow {}^{28}\mathrm{Si} + {}^{24}\mathrm{Mg}$, the broad component in $\Delta Z = 6$ from a 1α emission (the reaction $^{36}\mathrm{Ar} + {}^{16}\mathrm{O} \rightarrow {}^{28}\mathrm{Si} + {}^{20}\mathrm{Ne} + 1\alpha$) should be eight times bigger than this narrow part [Fig. 14(d)]. However, the experimental results show a rather small broad component, it is a factor of 10 too small to originate from ^{16}O. A similar argument applies for ^{12}C in the target [see Figs. 14(d) and 14(e)]; i.e., the broad distribution for $\Delta Z = 8$ is too small to be due to the $^{36}\mathrm{Ar} + {}^{12}\mathrm{C} \rightarrow {}^{48}\mathrm{Cr} \rightarrow {}^{28}\mathrm{Si} + {}^{16}\mathrm{O} + 1\alpha$ reaction. A maximum contribution of 15% to the narrow component in $\Delta Z = 6$ is estimated.

3. Analysis of the systematics of the widths of the out-of-plane distributions for the binary decays with sequential α emission. The broad out-of-plane correlations are expected to have an increasing width for increasing missing charges. This is indeed fulfilled for the distributions with missing charges of $\Delta Z = 2$, $\Delta Z = 4, 6$, and $\Delta Z = 8$; the width increases from 9° to 25°, respectively, as shown in Figs. 13 and 14. This fact shows that the observed broad components are due to the $^{36}\mathrm{Ar} + {}^{24}\mathrm{Mg} \rightarrow {}^{28}\mathrm{Si} + {}^{24}\mathrm{Mg} + \mathrm{X}\alpha$ reaction, where the $X\alpha$ particles are emitted from excited fragments.

4. Analysis of the in-plane angular distributions ($\theta_3 - \theta_4$). The analysis of these two-dimensional correlations was done together with kinematic calculations for the reactions, where the targets are either ^{16}O or ^{24}Mg. Using a gate applied in the TKE-out-of-plane correlation, we took only those events that produced the narrow part. Then, the kinematic curves for the same fragments ($Z_3 = 14$, $Z_4 = 12$), formed either in the $^{36}\mathrm{Ar} + {}^{16}\mathrm{O}$ or $^{36}\mathrm{Ar} + {}^{24}\mathrm{Mg}$ reactions were calculated. We used an appropriate excitation energy E_{ex} of the fragments to allow α-particle evaporation. For the $^{36}\mathrm{Ar} + {}^{16}\mathrm{O}$ reaction with $Q_{\mathrm{eff}} = 10$ MeV, with $Q_{\mathrm{eff}} = Q_0 + E_{\mathrm{ex}}$, the value for E_{ex} must be chosen to be below the decay threshold, but allowing mutual excitation. The latter kinematic curve lies in the border region of the experimental events in the two-dimensional angular distribution for the narrow part with $\Delta Z = 4$, see Fig. 15. In the region with a further increase of the excitation energy ($Q_{\mathrm{eff}} = 20$ MeV), fragments will emit α particles, and the experimental yield of the θ_3 vs θ_4 distribution can no longer

correspond to the exit channel ($Z_3 = 14$, $Z_4 = 12$) with a ^{16}O target. Thus the main yield originates from the ^{24}Mg target, for which we do not have restrictions in the excitation energy, i.e., from a reaction channel with the excitation energy sufficiently high in each fragment to allow evaporation of two α particles ($Q_{\text{eff}} \approx 36$ MeV). For this reaction, the kinematic curve is in good agreement with the region where the main intensity of the registered events are located.

5. Analysis of the out-of-plane correlations for the cases with odd total charges, such as the ($^{36}\text{Ar} + ^{24}\text{Mg} \rightarrow Z_3 + Z_4 + 1p + x\alpha$) channels, see Fig. 16. Here also an increase of the width as in Fig. 13 with increasing charge loss is expected. However, the channel ($-1p$, -2α) has the same width as the ($-1p$) channel (see Fig. 15 bottom and top rows). Because of this observation, it cannot originate from the reaction on the ^{24}Mg target, which actually has a very unfavorable Q value, and only a small cross section is expected. We can conclude that these events originate from the ^{16}O contaminant, because the corresponding Q values for the ($^{36}\text{Ar} + ^{16}\text{O} \rightarrow Z_3 + Z_4 + 1p$) reaction on ^{16}O are only (-10, -14) MeV, and the reaction with $1p$ evaporation can proceed without hindrance (see Fig. 4). With this observation and making the assumption that the binary fission channels of ^{60}Zn and ^{52}Fe with the evaporation of one proton are equal, we can determine a thickness of 16.8 μg/cm^2 (17%) of ^{16}O in the target. This result is in very good agreement with our previous determinations. From these estimations, we can also calculate the differential cross sections of the different exit channels of the reaction $^{36}\text{Ar} + ^{16}\text{O} \rightarrow Z_3 + Z_4 + 1p$, which are shown later in Fig. 21.

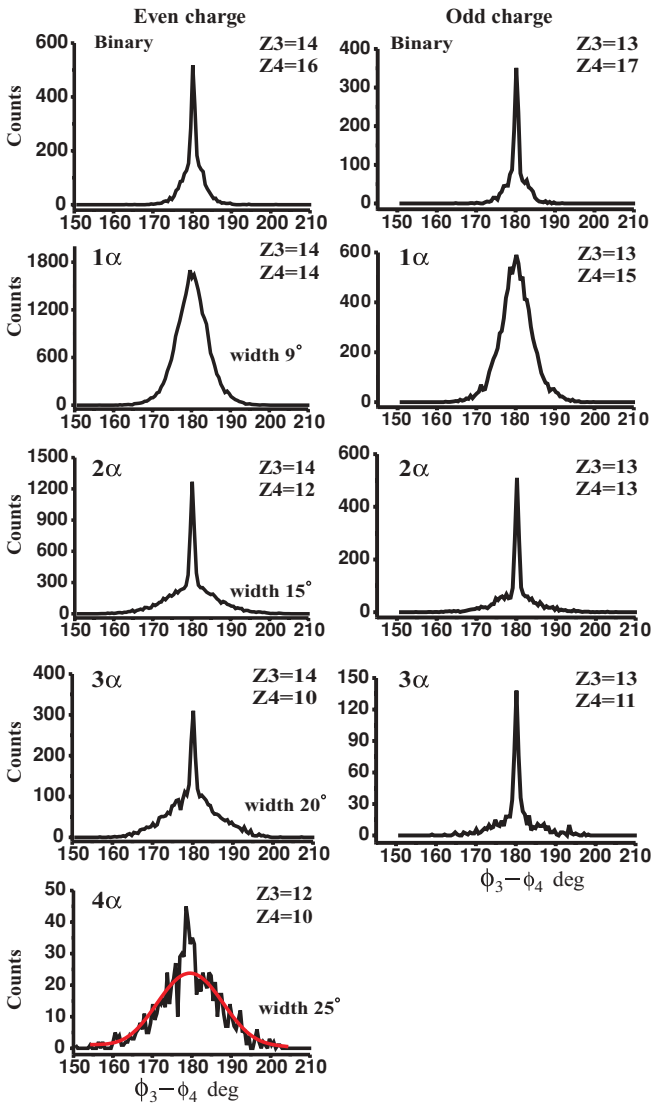

FIG. 13. (Color online) Yields $N(Z_3, Z_4)$ of coincident fragments with charges indicated by $Z3 + Z4$, as a function of the out-of-plane angles ($\phi_3 - \phi_4$) (in degrees). The widths (FWHM) of the angular correlations for the different fission channels are shown.

6. The higher kinetic energy of the narrow component. As discussed later (see Sec. V B), for the ternary decay the third fragments are assumed to be created in the neck and will have rather low kinetic energy in the center-of-mass system. We have performed calculations of the corresponding three-body decay. These cases imply, for example, that the missing particle, an ^{8}Be nucleus or ^{12}C, is emitted "backward" in a fast sequential decay from one of the moving heavier fragments.

For the statistical evaporation with all directions allowed, a "circular" broad distribution is obtained in the TKE vs ($\phi_3 - \phi_4$) plot. The collinear geometry gives us the upper energy limit of the TKE of these distributions. The resulting values of the TKE are in the range of 27–35 MeV higher than the center of the broad component of the energy distributions (see Fig. 24).

To summarize these observations, we conclude that the narrow yields originate predominantly from fission of ^{60}Zn (^{24}Mg target); approx. 15–17% of the narrow distributions can originate from target contaminants.

B. In-plane correlations, angular distributions

For $^{36}\text{Ar} + ^{24}\text{Mg}$, we show some angular distributions of the binary channels in Fig. 17. These differential cross sections can be obtained by taking either Det3 or Det4 as the primary gate, the corresponding symbols in the figure show these choices. In the range of the unrestricted efficiency of the coincident measurements, the angular distributions are rather flat and symmetric around 90°. This result points to the fact that the binary decay is a fission process from an equilibrated compound nucleus. For the fusion-fission mechanism, the angular distributions of the final fragments should be isotropic in the center-of-mass frame, with a rise toward small angles. A deviation from symmetry (and isotropy) will characterize processes with the formation of a dinucleus system, and a fixed direction for the emission of the fragments would arise in such processes.

Another feature, which can be used to characterize the reactions is the folding angles (θ_3, θ_4) correlations in the reaction plane of the two coincident fragments. The correlations in the (θ_3, θ_4) plane reflect the different geometric coincidence efficiencies of the BRS. For symmetric mass splits and corresponding (negative) Q values, the experimental choice of the angular ranges of the BRS covers perfectly the

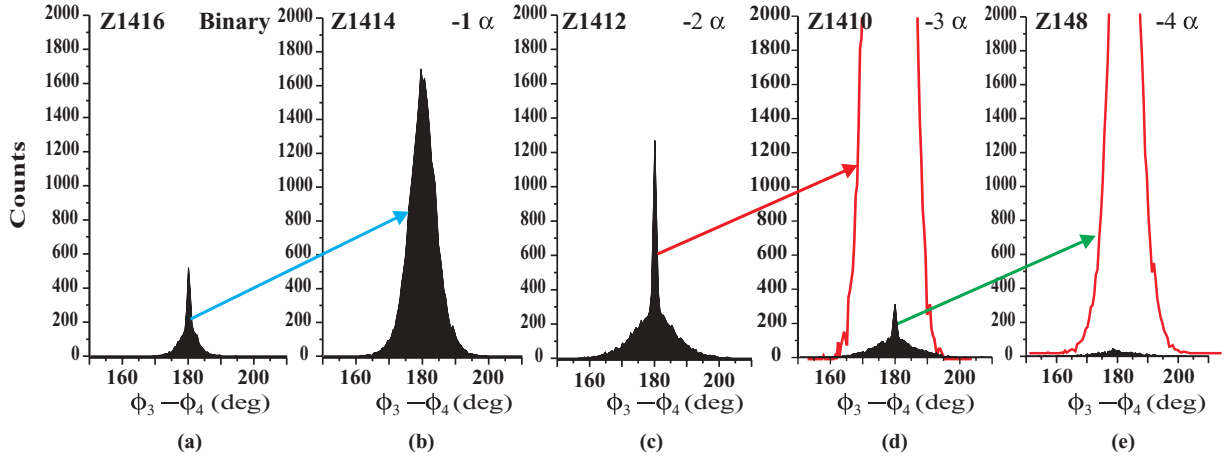

FIG. 14. (Color online) Out-of-plane angular ($\phi_3 - \phi_4$), in degrees, distributions for fission with definite values of $Z_3 + Z_4$, with calculations showing the expectation for the decays with -1α loss for ^{60}Zn, and the assumption of a narrow peak for ^{52}Fe from ^{16}O in the target and ^{48}Cr from ^{12}C, respectively. The respective wide components for the determination of the contributions from contaminants in the target are shown (see text for more details).

regions of interest. For more asymmetric mass splits, this region eventually moves out of the experimental (θ_3, θ_4) range; this is illustrated by the angular correlations in the Figs. 18 and 19.

Of further interest is the comparison with kinematic calculations of the observed binary coincidences, already mentioned before. For the [$Z_3 = 14$(Si) + $Z_4 = 12$(Mg)] channel shown in Fig. 16, the calculated kinematic lines are shown together with the kinematic lines for the reactions on ^{16}O, which is a binary channel. To have the possibility of two α particles evaporated, the corresponding excitation energy in the fragments should be added to the ground state Q values. Very negative Q values for the reaction on ^{24}Mg have to be assumed ($Q_{\rm eff} = Q_0 - 25$ MeV). The emission of the α particles corresponds to a broad region in the in-plane and out-of-plane angular distributions. As discussed before, a separation of events beyond the kinematic line for ^{16}O is possible, and the remaining events (the dominant part) are due to the ^{24}Mg target.

Summarizing all these conditions, we are able to extract the differential cross sections for binary (broad components) and ternary (narrow) fission yields.

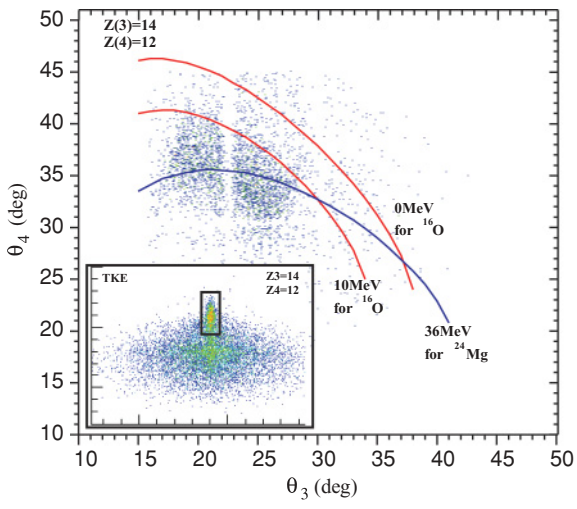

FIG. 15. (Color online) In-plane θ_4 vs θ_3 (in degrees) correlations of coincident fragments for the channels gated on the narrow (ternary) components for definite values $Z_3 + Z_4$ for the fission defined by $Z_3 + Z_4 + 2\alpha$. The kinematic calculations are shown for the Mg target and for the O target (channel $Z_3 + Z_4 + 0\alpha$ representing a binary channel) with the effective Q values as indicated and as discussed in the text. The angular range in the center-of-mass frame is between $\theta_{\rm c.m.} = 65^\circ$ and 120°.

C. Differential cross sections

As shown in the previous section, the angular distributions are rather flat, therefore we can give average values of the differential cross sections for the different exclusive binary and ternary channels in the range of the observed center-of-mass angles $\theta_{\rm c.m.}$. These ranges are approximately from 65° to 120° with a variation of 10°, depending on the values of (Z_3, Z_4). We have plotted the yields (differential cross sections) of the broad distributions for the exclusive binary fission channels in Fig. 20 (left panel) and for the ternary fission (right panel). The yields have been analyzed as a function of charge asymmetry for the different values of missing charges (ΔZ, ΔZ = even). In Fig. 20, the charges of the fragments registered in Det3 are plotted on the x axis. The fragments in the Det4 should be $Z_4 = Z_{\rm CN} - Z_3 - \Delta Z$. Similarly, the yields for $\Delta Z =$ odd, i.e., for the processes with emission of $1p$, $1p + 1\alpha$, and $1p + 2\alpha$, are given in Fig. 21. There the exclusive differential cross sections for the ^{24}Mg target are shown together with the differential cross sections for the elements produced from the reaction on ^{16}O in the target. We repeat our result, that 17%; contributions of reactions on ^{16}O (as contaminant in the target) are contained in the values shown in Fig. 20.

The yields as a function of the charge asymmetry should be symmetric around the value $(Z_3 + Z_4)/2$ for either combination of (Z_3, Z_4). This symmetry is well respected except for the larger asymmetries, where deviations by a factor of

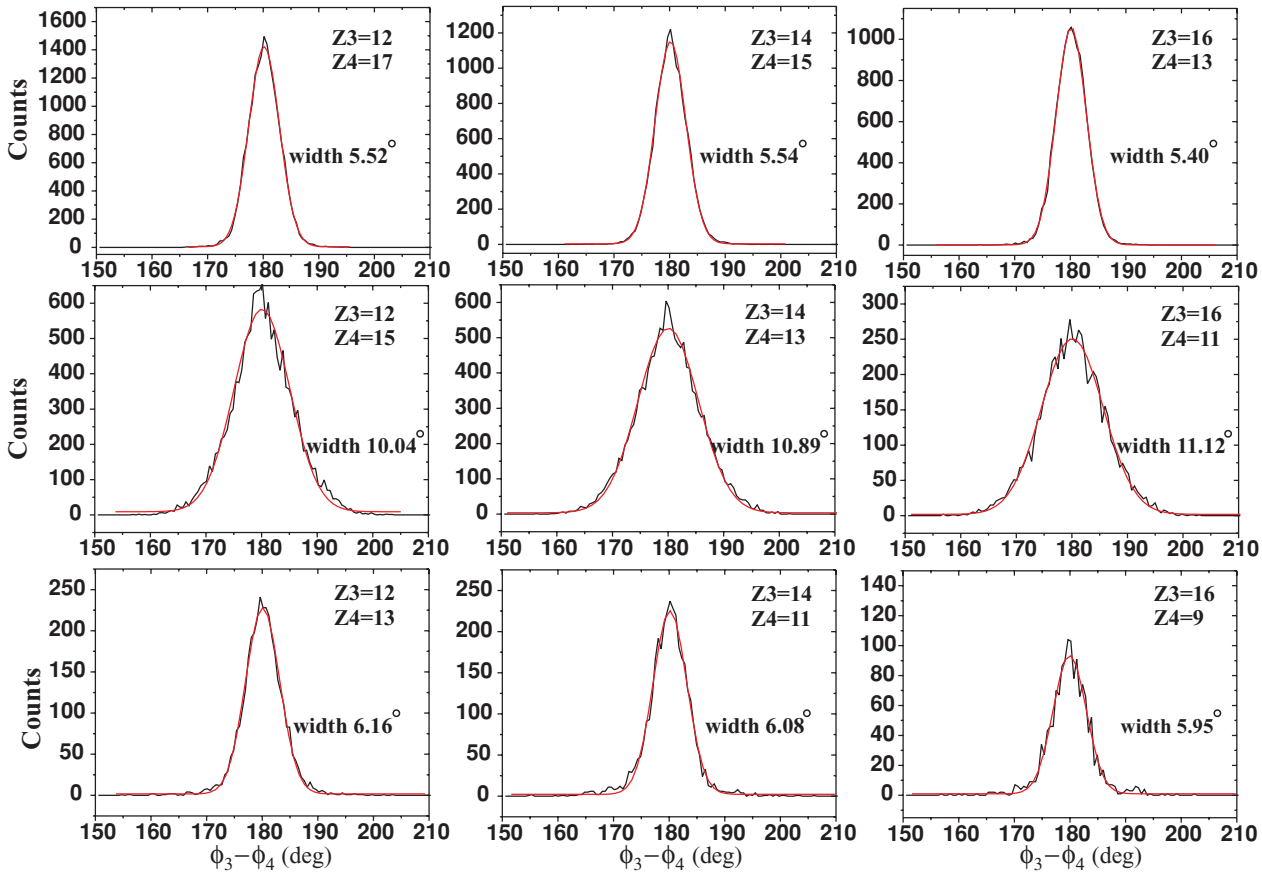

FIG. 16. (Color online) Out-of-plane angular ($\phi_3 - \phi_4$), in degrees, distributions for coincident fragments with charges ($Z_3 + Z_4 =$ odd), indicated as ($Z3$, $Z4$). Top row: the process with $1p$ emission; middle row: $1p + 1\alpha$ emission; bottom row: $1p + 2\alpha$ emission. The Gaussian fit functions and the widths (FWHM) of the angular correlations are indicated.

1.5–2 appear owing to reduced kinematic efficiencies and differences in setting gates at the low E values. The result shows that the efficiencies and the gates chosen in the data reduction correspond to the same energy ranges. We also note that the absolute values of the cross sections of the present work are almost the same (factors 1.5–2) as those obtained in the independent experiment with the BRS-Euroball setup for the fission decay of ^{56}Ni in the ^{32}S + ^{24}Mg reaction (the values of the angular momentum and excitation energy are similar) [20,21]. The inclusive and exclusive cross sections are summarized in a histogram in Fig. 22.

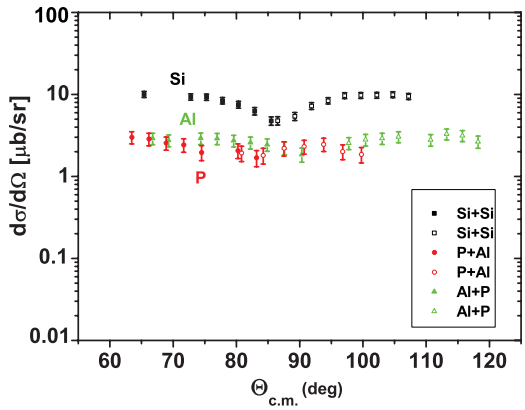

FIG. 17. (Color online) Differential cross sections for coincident fragments for some channels (defined by $Z_3 + Z_4 + 1\alpha$) representing the binary fission (broad) components. The angular ranges in the center-of-mass frame are between $\theta_{c.m.} = 65^\circ$ and 120°.

V. INTERPRETATION, TERNARY FISSION

A. Reaction mechanisms

Before we explore the interpretation of the data as compound nucleus decay, we briefly discuss a few other reaction mechanisms for the binary and ternary cluster decay. Most important in the present work are the out-of-plane correlations for events that cover a large angular range in ϕ and θ. This was only possible thanks to the large solid angle of the BRS and its high spacial resolution in the x and y coordinates. The broad component in the out-of-plane distributions with $\Delta Z = 2$–8 can be understood as a statistical α-emission process where 1–4α particles are emitted from the fully accelerated fragments. In the momentum space, the fragments after emission have a kinematic angular cone of the scattering. The mechanism of this process has been shown schematically in Fig. 8. The narrow components around $(\phi_3 - \phi_4) = 180^\circ$ can originate from different fission mechanisms:

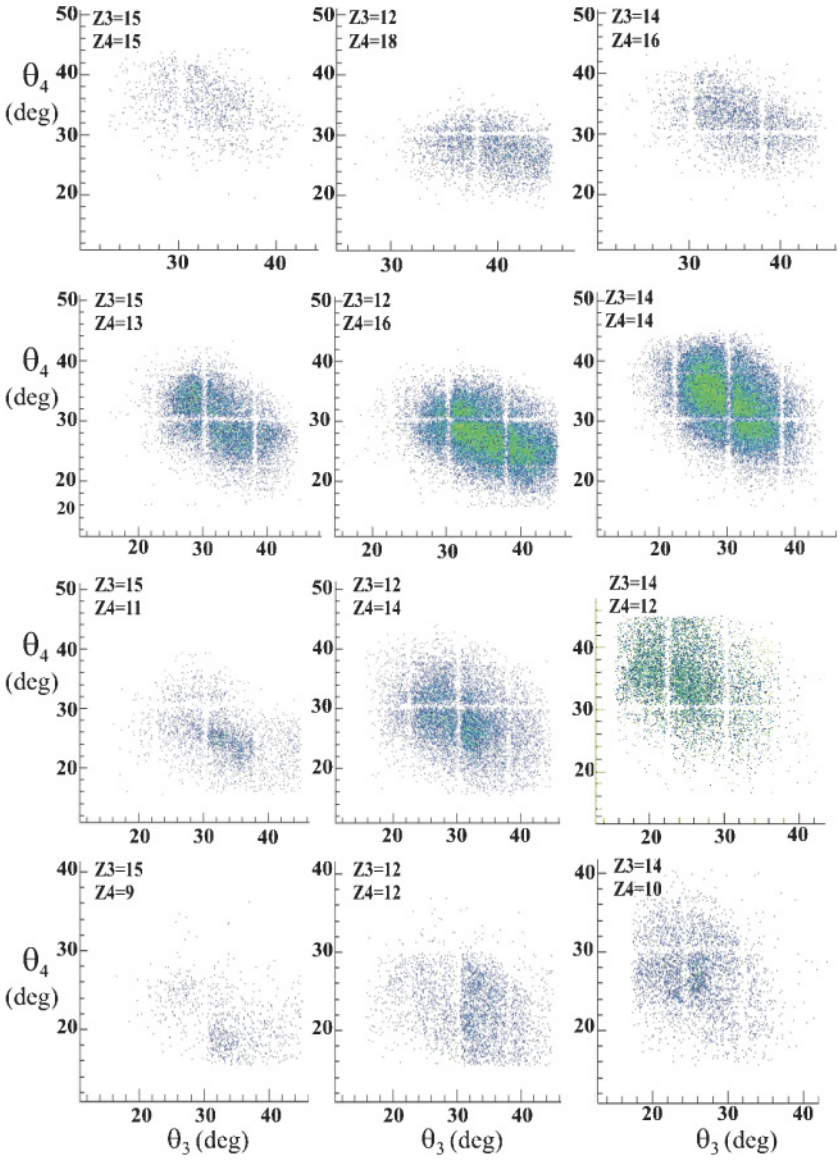

FIG. 18. (Color online) Correlations of the in-plane angles (θ_3, θ_4) (in degrees) for coincident fragments with charges indicated as Z_3, Z_4, for $^{36}\mathrm{Ar} + {}^{24}\mathrm{Mg}$ at $E_{\mathrm{lab}} = 195$ MeV. The empty regions are due to gaps in the electronically defined readout.

(i) A fission process after the fast emission of, for example, one or two (or even more) α particles, a process that will slightly disturb the observed correlation of the two subsequently emitted fission fragments (prefission emission).

(ii) A mechanism where, e.g., four charge units (the case of two missing α particles) must be emitted, correlated in-plane by a process involving two primary heavy ejectiles, with their angular momenta strongly aligned perpendicular to the reaction plane.

(iii) Ternary fission with the "emission" of the missing charges from the neck, the missing mass ($X\alpha$ particles) is emitted backward (in a sequential process, see below) in the center-of-mass frame. This process produces a narrow (ϕ_3, ϕ_4) correlation as in a standard binary decay, because the neck particles carry small momentum perpendicular to the reaction plane. The emission angle $(\phi_3 - \phi_4)$ remains 180°; this process can define coplanar or collinear decays (see Fig. 8).

For the case (i), we have to evaluate the second chance fission probability. One can use the values of the evaporation cross sections from the detailed analysis of the CN decay which has been done by Sanders *et al.* [11]. The CN decays are mainly by particle evaporation, giving rise to dominantly residual masses of $A = 48$–50 (emission of one or two α particles and some nucleons). This result is consistent with the systematics of Morgenstern [26], that the average energy needed to emit one nucleon is 16.4 MeV and for one α particle is 23.4 MeV. Similarly, in the emission of one fast (preequilibrium) α particle, this amount of energy or more will be removed. For binary fission to occur after the emission of a first particle, the fission probability is decreased drastically, because of the reduced excitation energy, and no second chance fission can be expected in such a reaction. Indeed no significant contribution from a narrow peak in the (ϕ_3, ϕ_4) correlations are observed for the fragment-fragment coincidences with one missing α particle ($\Delta Z = 2$) or one missing charge ($\Delta Z = 1$). The arguments against the role of prescission α particles are even more severe in the cases of two prefission α particles, and we can rule out this process.

For scenario (ii) involving a correlated emission of the α particles from the two fragments, we can argue as follows.

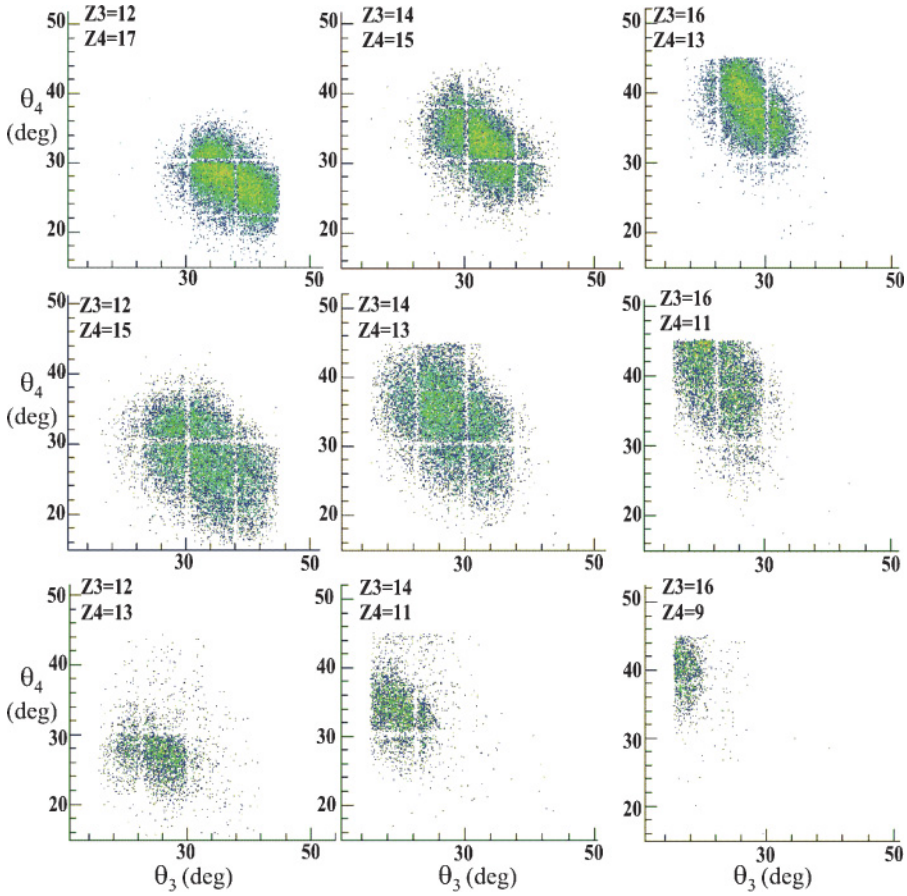

FIG. 19. (Color online) In-plane experimental angle-angle correlations of fragments for channels of binary coincident fission events defined by $(Z_3 + Z_4 + 1p + x\alpha)$. The center-of-mass angular ranges are between $\theta_{\text{c.m.}} = 65^\circ$ and 120°.

The fact that the narrow correlations appear as strong for $\Delta Z = 4$ and 6 makes it rather unlikely that such a very special correlation persists through all decays. The correlation created in the first binary decay must be complete and has to persist in the sequence of secondary emissions from the fragments for an odd and even number of emitted α particles.

For the third scenario, we assume a ternary fission process with the third clustered fragment in the neck (which will consist of α particles). If the two heavier fragments are emitted in a coplanar (or collinear) geometry with the third fragment, a correlation as sharp as in the case of a binary fission process is expected. This will happen naturally for the highest angular momenta, and only in these does the condition for the height of the saddle points allow a competition between ternary and binary decays, as shown in Sec. V B. Only this scenario can give a consistent image of the observed decay characteristics.

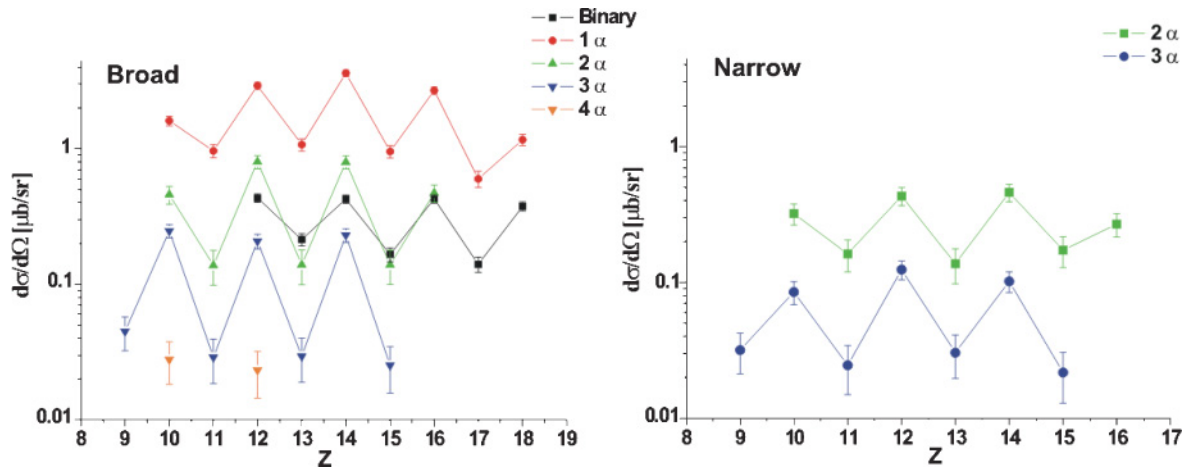

FIG. 20. (Color online) Differential cross sections in the reaction ^{36}Ar + ^{24}Mg for channels defined by $(Z_3 + Z_4 + x\alpha)$ of the broad (binary) and narrow (ternary) components of the coincident fission fragments. They represent the average over the angular range $\theta_{\text{c.m.}} = 65^\circ$–$120^\circ$ in the center-of-mass system. The fission channels with missing 1α, 2α, 3α, and 4α particles are shown.

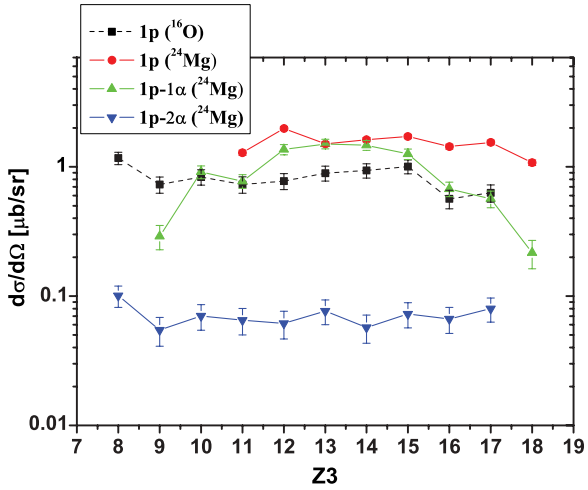

FIG. 21. (Color online) Differential cross sections for the reaction ^{36}Ar + ^{24}Mg as in Fig. 20 for channels defined by $Z_3 + Z_4 + 1p + x\alpha$, and the differential cross section in the reaction ^{36}Ar + ^{16}O for channels defined by $Z_3 + Z_4 + 1p$. The fission channels with missing $-1p$, $(-1p, -1\alpha)$, and $(-1p, -2\alpha)$ for ^{24}Mg target and $-1p$ for ^{16}O target are shown.

B. Kinematics of binary and ternary fission

For the discussion of the ternary fission mechanism, we will consider the formation and decay of the compound nucleus at the highest angular momenta, as also discussed in Ref. [27]. In this work, a three-cluster system with an interaction potential between the clusters as obtained from the experimental data is considered, and it is shown that for the small angular momenta a triangular configuration is favored. For higher angular momenta, the decay system has a stretched configuration caused by centrifugal forces. For the ternary cluster decay in a three-body configuration at high angular momentum, the energy is minimized if the lighter fragment is placed between of the two heavier fragments. The collinear configuration has the highest moment of inertia and the lowest energy for the saddle point. This fact produces the narrow

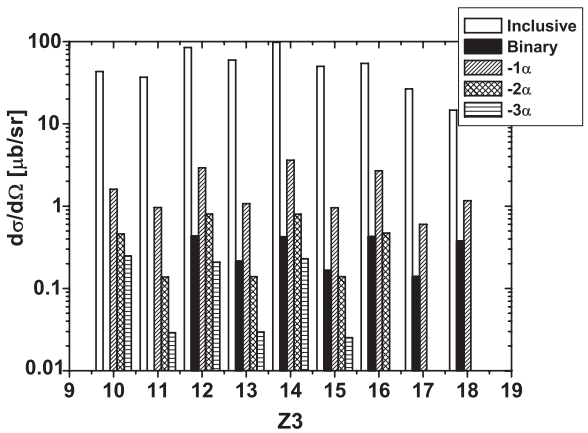

FIG. 22. Inclusive (open histogram) and exclusive (solid and shaded histograms) diferential cross sections for fission (in the angular range $\theta_{\text{c.m.}} = 65^\circ$ to 120°) in the ^{36}Ar + ^{24}Mg reaction.

component in the ϕ correlations at $(\phi_3 - \phi_4) = 180^\circ$. The distinction between the broad and narrow components can be viewed as due to two different time scales of the ternary cluster decay. For the broad component, the secondary cluster emission occurs after the two heavier fragments have been accelerated by the decay energy (Coulomb and centrifugal potentials). The narrow component is obtained if in the fission process two neck ruptures occur in a short time sequence.

As a model calculation for ternary fission we will discuss the decay of the CN ^{60}Zn with 2α or 3α clusters formed in the neck. This decay proceeds through two phases. First is the decay of the compound system into two highly excited fragments. We actually may assume a population of the resonant cluster states in these fragments. The second step is the sequential emission of the ternary fragment (α clusters, cluster c), from one of the fragments. We write schematically the reaction as $A + a \to B + (b + c)$, see Fig. 23, with the fragments B and b finally observed. The collinear decay mechanism can be modeled with the α clusters being emitted "backward" in the second step in a very short time sequence, comparable to the fission time. In this case, we will assume that the primary angle between fragments b and B remains 180° in the center-of-mass frame, as shown in Fig. 23(b). In the alternative decay with the statistical emission of two or three α clusters from highly excited fragments, the primary emission angle is changed into an emission cone (see Fig. 8), due to the recoil momentum induced by the α clusters. The *average* value of the angle would not change, as well as the average momentum, giving an average value of TKE corresponding to the total Q value (Q_{eff}). We note that for the statistical decay, in addition to the ground state Q value, an excitation energy in the primary fragment sufficiently high above the Coulomb barrier for the emission is needed. In the following, we discuss the kinematics of the ternary decay.

As an example, we take the 2α-emission process, and we perform our calculations in the center-of-mass frame of the compound nucleus. We define $\vec{P}_B$, $\vec{P}_{bc}$, $\vec{P}_b$, and $\vec{P}_c$ as the momenta of the first primary fragment B, of the second primary fragment bc, of the final fragment b (after cluster emission), and of the ternary cluster c, correspondingly. Analogously we define E_B, E_{bc}, E_b, and E_c as the kinetic energies in the exit channel.

For the first phase of the reaction, energy and momentum conservation gives, with

$$Q_{\text{eff}} = Q_0 + E^*, \quad \vec{P}_B + \vec{P}_{bc} = 0,$$

or

$$\begin{cases} E_B + E_{bc} = E_{\text{c.m.}} + Q_{\text{eff}}, \\ m(B)E_B = m(bc)E_{bc}. \end{cases}$$

From here we define the energy of the two fragments

$$E_B = \frac{m(bc)[E_{\text{c.m.}} + Q_{\text{eff}}]}{m(bc) + m(B)}, \tag{2}$$

$$E_{bc} = \frac{m(B)[E_{\text{c.m.}} + Q_{\text{eff}}]}{m(bc) + m(B)}. \tag{3}$$

In the second phase, when α clusters are emitted from the fragment bc [see Figs. 23(b) and 23(c)], the three-body

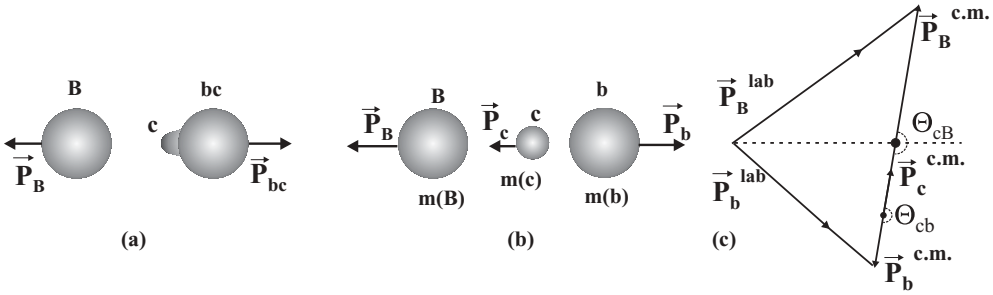

FIG. 23. Sequential fission decay: Ternary fission as a consecutive fast two-step process. The first step - (a), a binary decay of the hyper deformed compound system in two fragments $B + (b + c)$. The second step - (b) - the decay of $(b + c)$, cluster C emission from one of the fragments, (c) the vectors in the laboratory and the center of mass systems. The configuration is assumed to be collinear at high angular momentum.

kinematics in the center-of-mass frame for the collinear cluster decay of the compound system ^{60}Zn has to be calculated. Energy conservation for this reaction gives $E_B + E_b + E_c = E_{\text{c.m.}} + Q_{\text{eff}}$. The conservation of the linear momentum gives

$$\vec{P}_B + \vec{P}_b + \vec{P}_c = 0. \tag{4}$$

The kinetic energy of one of the fragments is then

$$E_b = \frac{(\vec{P}_B + \vec{P}_c)^2}{2m(b)} = \frac{\vec{P}_B{}^2 + \vec{P}_c{}^2 + 2\vec{P}_B\vec{P}_c}{2m(b)} = \frac{m(B)}{m(b)}E_B + \frac{m(c)}{m(b)}E_c + \frac{2\sqrt{m(B)m(c)}}{m(b)}\sqrt{E_B E_c}\cos\theta_{Bc}, \tag{5}$$

where θ_{Bc} is the angle between $\vec{P}_B$ and $\vec{P}_c$; in our case, $\cos\theta_{\text{Bc}} = 1$. The equation in velocity units is

$$E_b = \frac{m^2(B)}{2m(b)}\upsilon_B^2 + \frac{m^2(c)}{2m(b)}\upsilon_c^2 + \frac{2m(B)m(c)}{m(b)}\upsilon_c\upsilon_B. \tag{6}$$

The velocities υ_B, υ_c have been calculated. For the definition of υ_c we consider the decay of the primary fragment bc into fragment b and cluster c. Then the conservation of the linear momentum for this case is $\vec{P}_b = -\vec{P}_c$. For the energy, we have $E_c + E_b = E^*_{bc}$, where $E^*_{bc} = E^{\text{c.m.}}_{bc} + Q$, the excitation energy of fragment bc. The energy of c is

$$E_c = \frac{m(b)[E^*_{bc}]}{m(b) + m(c)},$$

and from here we define υ_c.

The calculations have been carried out for the case $^{36}\text{Ar} + {}^{24}\text{Mg} \rightarrow {}^{60}\text{Zn}^* \rightarrow {}^{24}\text{Mg} + {}^{36}\text{Ar}^* \rightarrow {}^{24}\text{Mg} + {}^{28}\text{Si} + 2\alpha$. From the calculations, we find that in the above-mentioned model for ternary fission as a sequential process, the TKE values are larger than the average value of the TKE of the fragments produced in the binary decay processes with the random emission of α particles from the moving fragments. In fact, we expect that the ternary fission process produces energies of fragments b, which are placed at the upper limit of the almost "circular" distributions of the TKE-(ϕ_3, ϕ_4) correlations (see Fig. 11).

For the narrow part in the out-of-plane correlations, we can compare the result of the calculations with the experimental data. The energy in the experimental data was obtained in the laboratory system, but the difference between the TKE of the ternary fission and of the energies after the α evaporation processes can be compared with calculations for the TKE in the center-of-mass frame. Using gates G1 (see Fig. 24), we have separated the narrow and broad components in the experimental data and have observed that the average difference of TKE between the narrow and the broad parts is (for $c = 2\alpha$) approximately 27 MeV, see Fig. 24, top right. This value agrees with the calculations where the difference is 30 MeV. The experimental relative values have an uncertainty of 1 MeV, as discussed in Sec. III B. In the same way, calculations were performed for the ternary 3α-cluster decay: $^{36}\text{Ar} + {}^{24}\text{Mg} \rightarrow {}^{24}\text{Mg} + {}^{24}\text{Mg} + 3\alpha$. We predict that the TKE of the fragments are 33 MeV higher than the average value in the binary decay with statistical 3α emission from fragments. This is again in good agreement with the experimental result. The experimental difference is 31 MeV, see Fig. 24, bottom right. To check that this result does not depend strongly on the lower border of the gates, we opened the gate to the lower TKE values (see Fig. 24, G2). The average difference of TKE between the whole narrow and the broad parts has remained the same (actually the counting rate around the peaks did not change, differences smaller than 100 keV) as it was before (using G1). Therefore, the dominant yield in the data is concentrated in the chosen gates. From these results, we conclude that the collinear geometry describes the the TKE-(ϕ_3, ϕ_4) correlations in an appropriate way. The experimentally wide distributions in TKE actually suggest that there is also a large component of ternary cluster decay with coplanar geometry with the collinearity as the limiting case. This may be connected to a distribution of fission times, as suggested in Sec. V C.

As a final statement, we may consider that the final fragments B and b in the case of a ternary cluster decay should have rather low excitation energy (i.e., they are "cold" fragments) as compared to the binary case. In contrast, for the latter case, as expected from the statistical phase-space considerations (see below), the highest possible excitation energy (with the maximum of level densities) of the primary fragments is populated, and a feeding into a high level density after particle emission is expected also in the final fragments.

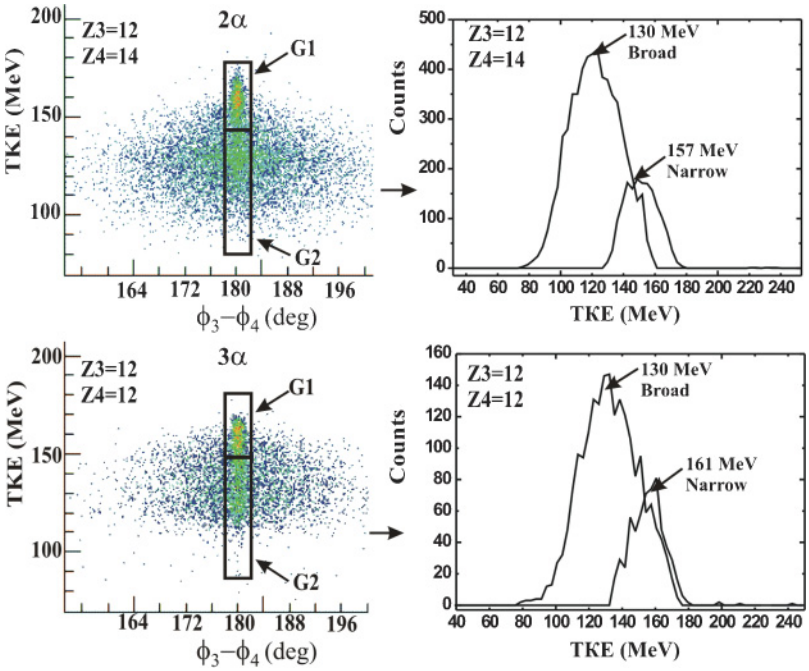

FIG. 24. (Color online) Left: two-dimensional TKE distributions vs out-of-plane angles (in degrees) ($\phi_3 - \phi_4$). Right: projection of the TKE with two separated broad and narrow components (by using gate 1, G1). Gate 2 (G2) is for the checking procedure, see text for details.

C. Statistical model fission decay

From the present experimental results, we conclude that the cluster decay of an equilibrated CN is observed. A main point in the interpretation of the data is to explain the observed yield of the "ternary" fission channels relative to the binary decay. The basic Q values for the ternary mass split and the corresponding evaporation process are the same; however, for the evaporation to occur, the fragment must be excited to a higher energy above the separation energy; namely, the corresponding Coulomb barriers should be included. This makes the $Q_{\rm eff}$ for the statistical evaporation 10 MeV higher (or more), and in the statistical model an advantage for the direct ternary mass split may occur.

For the interpretation of the data as a fission process, we have to consider the statistical phase space for both binary and coplanar ternary fission. This can be achieved by the extended Hauser-Feshbach method (EHFM) [28], which has been developed for heavy-ion fusion-fission reactions to provide a detailed analysis of all the possible decay channels by including the fusion-fission phase space. The EHFM supposes that the fission probability is proportional to the available "phase space at the scission point." The narrow width and the high values of the TKE of ternary events give us opportunity to make a model in which the formation of $N\alpha$ particles in the neck is assumed. We will disregard the phase space of the particles in the neck, as well as their kinetic energy. The initial stages for the ternary and binary fission may be considered to be the same, the difference being in the time scales of the separation of the ternary clusters, which are emitted earlier in a coplanar or collinear configuration. Energy conservation then gives

$$E^*_{\rm CN} = Q_{\rm tern} + (U_3 + U_4 - E_{3,4})$$

for a compound nucleus (CN) of an excitation energy $E^*_{\rm CN}$, with a ternary Q value $Q_{\rm tern}$. The excitation energies of the fragments are given by U_3, U_4 with their relative kinetic energy as $E_{3,4}$.

The differential decay cross section for different mass partitions (i, j) will depend on the product of the level densities $\rho_i(U_i, J_i)$, for $i = 3$, $j = 4$ of the fragments and the total inverse fusion cross section $\sigma(E_{i,j}, R_s, J)$, that is,

$$\frac{d\sigma(i,j)}{d\Omega\, dE_k(i,j)} = C\rho_1(U_i, J_i)\rho_2(U_j, J_j)\sigma(E_{3,4}, R_s, J).$$

We use $J = J_3 + J_4$, for the spins of the fragments, with total spin J. The radial variable R_s ($R_s = R_3 + R_4 + d$, where d is a neck parameter) stands here for the shape of the saddle, and we defined the "inverse" formation probability $\sigma(E_{3,4}, R_s, J)$ as in the usual fission theory, where it belongs to the corresponding fusion cross section. We have the constraints for the excitation energies and the kinetic energy: $U_3 + U_4 = E^*_{\rm CN} - Q_{\rm tern,3,4} - E_{3,4}$. Or expressed as an effective Q value, $Q_{\rm eff,3,4} = Q_{\rm tern,3,4} + U_3 + U_4$. In the ternary decay, the two excitation energies of both heavy fragments (3,4), which are registered in coincidence before further decay, must have values $U_{3,4}$ below their α-decay threshold. In our case for even-even fragments with $N = Z$, the thresholds for an evaporation process (including a Coulomb barrier) are in the region of (10–15 MeV). In the statistical model, see, e.g., Ref. [11], the spin-dependent level densities in the two fragments are determined by their excitation energies. The effective Q values are very important and determine the relative kinetic energy $E_{\rm kin}(i, j) = E_{3,4}$ and thus the corresponding penetrabilities $T(E_{\rm kin}(i, j), R_s, J)$. For these the potential energy surfaces for the two fragments must be considered. The formation cross section in the exit channel, $\sigma(E_{\rm kin}(i, j), R_s, J)$, for a given $E^*_{\rm CN}$ and J contains the different penetrabilities $T(E_{\rm kin}(i, j), R_s, J)$ in the exit channels, and we make the model assumption of an inverse

fusion given by

$$\sigma(E^*_{\rm CN}, J, Q_{\rm tern}, (i, j)) = \int dE_{\rm kin}\delta U\, d\Omega \frac{d\sigma}{d\Omega\, \delta U\, dE_{\rm kin}} \quad (7)$$

with $\delta U = U_3 - U_4$, which defines the excitation energy differences for the two fragments. The value of σ is thus strongly influenced by the ternary Q values of the channels (i, j). For the determination of $T(E_{\rm kin}(i, j), R_s, J)$, the potential energy surfaces of the fission path leading to the fission saddle point have to be evaluated.

At this point, a comment on the geometrical shape of the fission saddle and the three-body configuration is needed. The three fragments could be placed at different relative orientations; however, it can easily be shown that for larger values of the total spin J, the collinear configuration having the largest moment on inertia relative to all others will have the lowest barrier. This feature has been calculated for some specific orientations of the three fragments by Wiebecke and Zhukov [27], where it is shown that the lowest barrier occurs for the collinear configuration. Thus we may indeed expect the collinear ternary cluster decay, and the competition between binary and ternary fission becomes visible only at higher angular momenta.

For the total energy balance which includes these potential energies and their dependence of the rotational energy due to the deformed shape, we introduce the free energy $(i, j = 3, 4)$

$$E_{\rm free}(i, j) = E^*_{\rm CN} + Q_{\rm eff,3,4} + V^{\rm eff}_{\rm pot}(J, Z_3, Z_4, R_s). \quad (8)$$

The available free energy $E_{\rm free}(i, j)$ will be used to populate regions of maximum level density in the fragments, it will determine the yield for a particular partition. Most important is the total potential energy at the saddle point determined by $V_{\rm pot}(J, Z_3, Z_4, R_s)$. The latter contains the rotational energy $E_{\rm rot}(J, 3, 4, R_s)$, which depends on the total spin J and the moment of inertia $\Theta_{\rm ff}(R_s)$ and finally on the shell corrections $\Delta_{\rm sh}(R_s)$ expected for particular shapes at the deformed saddle point,

$$V^{\rm eff}_{\rm pot}(Z_3, Z_4, R_s) = E_{\rm rot}(J, 3, 4, R_s) + V_{\rm pot}(Z_3, Z_4, R_s) + \Delta_{\rm sh}(R_s). \quad (9)$$

The shell corrections $\Delta_{\rm sh}(R_s)$ for hyper-deformed shapes, which can be found in the review by Ragnarsson, Nilsson, and Sheline [7], are in the range of 3–8 MeV.

The energy available to populate states in the fragment can now be determined as in a binary configuration considering the potential energy surfaces as functions of deformation or fragment distances. To summarize, the positions of the fission barriers (and scission points) of different channels is governed by their Q values, by the liquid-drop energies, and by the rotational energies for a given J. These values are shown for some channels in Table I. Using this approach, the interpretation of the relative strength of the binary and ternary fission yields can be obtained. According to the statistical model, the differences between ternary and binary mass split arise from (a) different Q values, and therefore different barrier heights, but also different values of U_i, J_i, (b) total fission barrier heights due to the different moments of inertia $\Theta_{\rm ff}$ (see Table I), and (c) shell corrections for large deformations (with 2:1 and 3:1 axis ratios).

TABLE I. Q values, the inverse of the moments of inertia $(\hbar^2/2\Theta_{\rm ff})$ and the barrier heights (in MeV) for some fission channels for the ^{60}Zn compound nucleus.

Reaction	Q value (MeV)	$\hbar^2/2\Theta_{\rm ff}$	Barrier($J = 45$) (MeV)
Binary (-0α)			
^{32}S + ^{28}Si	+3.34	0.0330	70.5
^{30}P + ^{30}P	−3.76	0.0328	77.6
Binary (-1α)			
^{28}Si + ^{28}Si + 1α	−3.60	0.0149	55.2
^{30}P + ^{26}Al + 1α	−14.18		
Ternary (-2α)			
^{24}Mg + ^{28}Si + 2α	−13.58		68.5
^{26}Al + ^{26}Al + 2α	−24.59	0.0136	79.4
Ternary (-3α)			
^{24}Mg + ^{24}Mg + 3α	−23.57	0.0134	74.4
^{22}Na + ^{26}Al + 3α	−34.04		
Ternary (-4α)			
^{22}Na + ^{22}Na + 4α	−43.5	0.0140	90.1
^{16}O + ^{28}Si + 4α	−27.63		

In Table I we show for different binary and ternary fission channels, both the ground state Q values and the rotational energies at the saddle point for $J = 45\hbar$, which will determine the yields. For small values of J, the ternary fission probabilities are expected to be small, because they cannot compete with the other decay channels. The Q values for ternary mass splits attain large negative values. The effective excitation energies of the primary fragments in a binary decay before statistical emission (e.g., for 3α) must be rather higher, therefore the effective Q values are much larger than those quoted in the table.

Concerning the experimental odd-even effect in the binary yields, we find that the Q values for odd-odd charge fragments are typically 5–10 MeV more negative. In the same way, the odd-even effect with the lower yields of the ternary splits with odd charges can be understood, because less free energy is available with the increasingly negative Q values (up to $Z_{\rm CN}$-6) for the odd-Z fragments. These smaller yields are in accordance with the phase-space considerations and the penetrabilities. In these cases also less excitation energy in the two heavier fragments is expected, and less subsequent decays via particle evaporation. In fact, the narrow peaks in the $(\phi_3 - \phi_4)$ correlations dominate in the spectra if the sum of two odd charges (for $\Delta Z = 4, 6$) is taken (see Fig. 13).

The liquid-drop energies and the Q values, as well as the rotational energy, constitute the main part of the barrier height for the fission process. For the present reaction, these have been calculated by Royer [15], where the liquid-drop part of the potential energies is determined within a generalized liquid-drop model using quasimolecular shapes. In the binary and ternary fission channels, the saddle point corresponds to clusters kept together by the proximity forces. For the relative position of the binary and ternary fission barriers, clearly the ternary fission barrier for low values of J is much higher, and no ternary fission can be observed. With the inclusion of

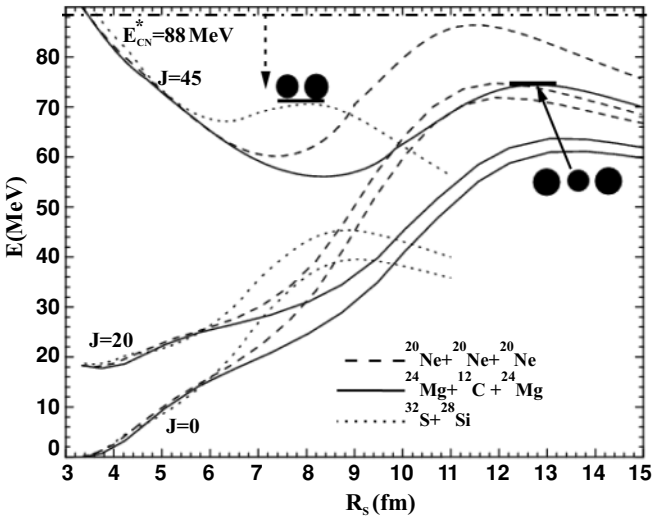

FIG. 25. Potential energies obtained in the liquid-drop model for selected fragmentations in the decay of ^{60}Zn as a function of the deformation (represented by the distance R_s between the two heavier fragments) for different angular momenta (in units of $\hbar$) for binary and ternary fission decay, respectively. Channels with different ΔZ (missing 0 and 3α particles) are shown.

the angular momentum, the rotational energy as a function of J increases much slower at the strongly deformed saddle point of the ternary mass split, as shown in Fig. 25. In this figure, three cases are shown: a symmetric ternary mass split, a ternary channel with a ^{12}C cluster in the center, and a binary channel. The difference relative to the binary mass split becomes smaller because of the differences in the moments of inertia Θ. From these calculations, we also notice that for the ternary fission process, the barrier is the highest for three equal mass fragments, whereas the barrier height decreases if the mass (and charge) of the "third" fragment in the neck region is smaller. Furthermore, the potential energy minima formed in the highly deformed rotating states are lower in the ternary valley than in the binary valley for large angular momenta.

Following these considerations, the ternary fission process can be found to favorably compete with the binary mass split at the highest angular momenta, at values around 42–45$\hbar$. An additional lowering of the barrier by deformed-shell corrections is predicted for large deformations in many calculations based mainly on the Nilsson-Strutinsky method [5]. These particular shapes of the hyper-deformation bring into play a deformed shell correction to the liquid-drop energy of approximately 5–10 MeV [7]. The ternary fission process from the hyper-deformed configuration can thus be further enhanced.

We summarize our result with the yield systematics shown in Fig. 20, where we can see a strong odd-even effect in both binary and ternary cluster decay (plotted as a function of the charge asymmetry). The experimental values are subject to some systematic errors, because the efficiency of the BRS-coincidence setup is only optimally suited for symmetric mass splits and for negative Q values of at least -20 MeV. For the most asymmetric mass splits, and less negative Q values, the experimental yields (as deduced from angle-angle, and energy-energy correlations) are sometimes reduced by 30%, because of cuts in the geometrical angular range or in the energy range. This effect is partially incorporated into the systematic errors given for the individual yields. In accordance with the statistical model expectations, we observe a maximum in the yields for the case of one missing α particle. In the binary mass split, at least one of the fragments has sufficient excitation energy for the evaporation of one α particle, making the channel ($Z_{\rm CN}$-2) the most intense. For all very negative Q values, the yields are lower and the fragments are expected to be rather "cold."

VI. CONCLUSIONS

We conclude that the observation in the out-of-plane correlations of the very narrow coplanar fission fragment coincidences is a unique feature, observed for the first time because of the unique detection efficiency of the BRS (see also Ref. [21] for the fission decay of ^{56}Ni). These data give clear evidence of the occurrence of ternary cluster decay processes. From our analysis we conclude that these must originate from the strongly (hyper) deformed states in nuclei with mass $A = 60$ formed at high angular momentum as predicted by Zhang *et al.* [3] as well as in the liquid-drop model of Ref. [1]. The neck of the fissioning nucleus, as calculated by Royer [15], represents a region of low nuclear density, which gives an additional reason for the favored formation of α clusters, an aspect which also has been discussed in the literature (see Ref. [29]).

The systematics of the yields shown in Fig. 20 confirm the expectations of the statistical model, i.e., that there is a strong odd-even effect in the yields (lower yields for the odd charges with more negative Q values) for all cases of the binary and the ternary cluster decays. A more detailed analysis based on the mentioned statistical decay model is in preparation.

The particles formed in the neck are expected to travel with the center-of-mass velocity in the beam direction (toward 0°). A corresponding measurement showing this phenomenon, one α particle from the neck in the decay of ^{28}Si into $^{12}\mathrm{C} + \alpha + {}^{12}\mathrm{C}$, has been reported by Scheurer *et al.* [30]. The present work also shows that the search for hyper-deformation in rapidly rotating nuclei, which has been done extensively using γ spectroscopy, should be pursued with charged-particle spectroscopy. For nuclei in the medium-mass region ($A = 40$–100), where the fissibility parameter is small, the formation of a longer neck is predicted [1]. For these cases, ternary cluster decays are expected. With three fragments, a complete reconstruction of the events can be undertaken with appropriate detector systems, which should include a zero degree hodoscope to detect the clusters formed in the neck. Such measurements offer the possibility of a precise spectroscopy of the extremely deformed states.

ACKNOWLEDGMENTS

We thank H. G. Bohlen, C. Wheldon, and T. Kokalova for their numerous discussions on this project. H. G. Bohlen has contributed to many aspects of this work. V. Zherebchevsky thanks the DAAD for its grant.

[1] S. Cohen, F. Plasil, and W. J. Swiatecki, Ann. Phys. (NY) **82**, 557 (1974).
[2] P. Moeller and R. Nix, Nucl. Phys. **A272**, 502 (1976).
[3] J. Zhang, A. C. Merchant, and W. D. M. Rae, Phys. Rev. C **49**, 562 (1994); W. D. M. Rae, J. Phys. Soc. Jpn. Suppl. **58**, 77 (1989).
[4] G. Leander and S. E. Larsson, Nucl. Phys. **A239**, 93 (1975).
[5] S. Aberg, H. Flocard, and W. Nazarewicz, Annu. Rev. Nucl. Sci. **40**, 439 (1990).
[6] S. Aberg and L. O. Joensson, Z. Phys. A **349**, 205 (1994).
[7] I. Ragnarsson, S. Aberg, and R. K. Sheline, Phys. Scr. **24**, 215 (1981); I. Ragnarsson, S. G. Nilsson, and R. K. Sheline, Phys. Rep. **45**, 1 (1978).
[8] S. J. Sanders *et al*., Phys. Rev. C **49**, 1016 (1994), and references therein.
[9] S. J. Sanders, D. G. Kovar, B. B. Back, C. Beck, B. K. Dichter, D. Henderson, R. V. F. Janssens, J. G. Keller, S. Kaufman, T.-F. Wang, B. Wilkins, and F. Videbaek, Phys. Rev. Lett. **59**, 2856 (1987).
[10] S. J. Sanders, D. G. Kovar, B. B. Back, C. Beck, D. J. Henderson, R. V. F. Janssens, T. F. Wang, and B. D. Wilkins, Phys. Rev. C **40**, 2091 (1989).
[11] S. J. Sanders, A. Szanto de Toledo, and C. Beck, Phys. Rep. **311**, 487 (1999), and references therein.
[12] Tz. Kokalova, W. von Oertzen, S. Torilov *et al*., Eur. Phys. J. A **23**, 19 (2005).
[13] A. V. Andreev, G. G. Adamian, N. V. Antonenko *et al*., Eur. Phys. J. A **30**, 579 (2006).
[14] G. Royer and F. Haddad, J. Phys. G **21**, 339 (1995).
[15] G. Royer, J. Phys. G **21** 249 (1995); G. Royer, F. Haddad, and J. Mignen, J. Phys. G **18**, 2015 (1992).
[16] A. St. Murphy *et al*., Phys. Rev. C **53**, 1963 (1996).
[17] S. Thummerer *et al*., Nuovo Cimento A **111**, 1077 (1998); Ph.D. thesis, Freie Universitaet, Berlin, 1999.
[18] V. I. Zherebchevsky, W. von Oertzen, D. Kamanin *et al*., Phys. Lett. **B646**, 12 (2007).
[19] V. I. Zherebchevsky, W. von Oertzen, and D. V. Kamanin, JETP Lett. **85**, N.3, 136 (2007); V. I. Zherebchevsky, Ph.D. thesis, St. Petersburg University, 2007.
[20] G. Efimov *et al*., Ph.D. thesis, Dubna University, 2008.
[21] W. von Oertzen, B. Gebauer, G. Efimov *et al*., Eur. Phys. J. A **36**, 279 (2008).
[22] B. Gebauer *et al*., in *Ancillary Detectors and Devices for Euroball*, edited by H. Grawe (GSI and the Euroball Ancillary Group, Darmstadt, 1998), p. 43; see also Achievements with the Euroball Spectrometer, 1997–2003, edited by W. Korten and S. Lunardi, p. 135 (unpublished).
[23] C. Beck *et al*., Nucl. Phys. **A734**, 453 (2004).
[24] B. Gebauer *et al*., in *Proceedings of the International Conference on the Future of Nuclear Spectroscopy, Crete, 1993,* edited by W. Gelletly *et al.* (NCSR Demokritos, Athens, 1994), p. 168.
[25] C. Beck and A. Szanto de Toledo, Phys. Rev. C **53**, 1989 (1996).
[26] H. Morgenstern *et al*., Z. Phys. A **313**, 39 (1983).
[27] H. J. Wiebecke and M. Zhukov, Nucl. Phys. **A351**, 321 (1981).
[28] T. Matsuse, C. Beck, R. Nouicer, and D. Mahboub, Phys. Rev. C **55**, 1380 (1997).
[29] H. Horiuchi, Nucl. Phys. **A731**, 329 (2004).
[30] J. N. Scheurer *et al*., Nucl. Phys. **A319**, 274 (1979).